Order Number 1352392

A comparison of thermal hydraulic models for pressurized water reactors

Stanley, Thomas Patrick, M.S.

The University of Arizona, 1993

U·M·I
300 N. Zeeb Rd.
Ann Arbor, MI 48106

A COMPARISON OF THERMAL HYDRAULIC MODELS FOR PRESSURIZED WATER REACTORS

by

Thomas Patrick Stanley

A Thesis Submitted to the Faculty of the

DEPARTMENT OF NUCLEAR ENGINEERING

In Partial Fulfillment of the Requirements
For the Degree of

MASTER OF SCIENCE

In the Graduate College

THE UNIVERSITY OF ARIZONA

1 9 9 3

STATEMENT BY AUTHOR

This Thesis has been submitted in partial fulfillment of requirements for an advanced degree at The University of Arizona and is deposited in the University Library to be made available to borrowers under rules of the Library.

Brief quotations from this thesis are allowable without special permission, provided that accurate acknowledgment of source is made. Requests for permission for extended quotation from or the reproduction of this manuscript in whole or in part may be granted by the head of the major department or the Dean of the Graduate College when in his or her judgment the proposed use of the material is in the interests of scholarship. In all other instances, however, permission must be obtained from the author.

SIGNED: Thomas P. Stanley

APPROVAL BY THESIS DIRECTOR

This thesis has been approved on the date shown below:

Robert L. Seale
Professor of Nuclear Engineering

4/21/93
Date

ACKNOWLEDGEMENTS

I would like to acknowledge the entire department of Nuclear Engineering at the University of Arizona for providing me with an outstanding undergraduate and graduate education.

I would also like to acknowledge the United States Navy for giving me the opportunity to attend graduate school.

My most sincere gratitude and appreciation goes to Dr. Phillip Secker whose countless hours, limitless patience and total dedication made this thesis possible.

To my mother and father:

who have made me what I am today.

To Cindy:

for her patience, understanding and support.

TABLE OF CONTENTS

LIST OF ILLUSTRATIONS 6

LIST OF TABLES 7

ABSTRACT 8

INTRODUCTION 9

METHOD 12

Palo Verde Nuclear Power Plant 14
CEPAC Computer Code Description 16
LASAN Computer Code Description 16
CEPAC-L Computer Code 17
Mass and Energy Calculations 18
Heat Transfer Calculations 22
Flow Rate Calculations 24
COBRA Computer Code 26
Correlations Used 27
Dynamic Moving Boundary Fuel Pin Model 30
Fluid Flow 31
Heat Transfer 35

RESULTS 44

Comparison of CEPAC-L to CEPAC 44
Steady State 44
Loss of ALL Primary Coolant Flow 52
Comparison of FUELPIN to COBRA 62
MDNBR versus Time 62
Position of MDNBR versus Time 67

DISCUSSION 73

APPENDIX A: PANDA Module Causality Diagrams 75

REFERENCES 85

LIST OF ILLUSTRATIONS

Figure 1. Palo Verde System-80 PWR 15
Figure 2. Single Channel Flow Regimes 32
Figure 3. Moving Boundary Model in a Boiling Channel . 33
Figure 4. Spacial Grid for Transient Conduction . . . 38
Figure 5. Loop Temperatures, Steady State 45
Figure 6. Pressurizer Level, Steady State 46
Figure 7. Pressurizer Pressure, Steady State 47
Figure 8. Steam and Feed Flows, Steady State 49
Figure 9. Steam Generator Level, Steady State 50
Figure 10. Steam Generator Pressure, Steady State . . . 51
Figure 11. Reactor Power, Loss of All Flow 53
Figure 12. Primary Coolant Flow, Loss of All Flow . . . 54
Figure 13. Loop Temperatures, Loss of All Flow 55
Figure 14. Pzr Pressure, Loss of All Flow 56
Figure 15. Pzr Level, Loss of All Flow 57
Figure 16. Steam and Feed Flows, Loss of All Flow . . . 58
Figure 17. Steam Generator Level, Loss of All Flow . . 60
Figure 18. SG Pressure, Loss of All Flow 61
Figure 19. Axial Heat Flux Profile 63
Figure 20. MDNBR vs Time, Loss of All Flow, BOL 64
Figure 21. MDNBR vs Time, Loss of All Flow, EOL 65
Figure 22. MDNBR vs Time, Loss of All Flow, MOL 68
Figure 23. Position of MDNBR vs Time, LOAF, BOL 69
Figure 24. Position of MDNBR vs Time, LOAF, MOL 70
Figure 25. Position of MDNBR vs Time, LOAF, EOL 71

LIST OF TABLES

Table 1. Palo Verde Nuclear Power Plant Data 14

Table 2. Correlations used by COBRA 29

Table 3. Correlations used by FUELPIN 34

ABSTRACT

This thesis compares a new dynamic moving boundary thermal hydraulics fuel pin model (FUELPIN) to a known thermal hydraulics code (COBRA) for the following relationships:

1) Minimum Departure from Nucleate Boiling Ratio (MDNBR) versus time for transient conditions in a Pressurized Water Reactor (PWR) channel, and
2) Position of Minimum DNBR versus time for transient conditions.

Relationships between MDNBR and position of MDNBR versus time were analyzed by comparing:

1) output of COBRA, a steady state thermal hydraulics model, with inputs from a PWR simulation code (CEPAC-L),
2) output of CEPAC-L linked FUELPIN.

CEPAC-L computer model was shown to be a good simulation of a PWR during steady state conditions and a loss of all primary coolant flow casualty by comparison with an accepted PWR simulation code (CEPAC). FUELPIN was shown to predict larger thermal margins than COBRA for loss of all primary coolant flow transients in PWRs.

INTRODUCTION

This thesis compares a new dynamic moving boundary thermal hydraulics fuel pin model (FUELPIN) to a known thermal hydraulics code for the following relationships:

1) Minimum Departure from Nucleate Boiling Ratio (MDNBR) versus time in a Pressurized Water Reactor (PWR) channel during transient conditions, and
2) Axial Position of MDNBR within the channel versus time for transient conditions.

In order to conduct this comparison a working simulation model of a PWR, that could be modified and adjusted, had to be installed at the University of Arizona. This model was then compared to an existing executable code to verify its accuracy and usefulness for simulation. The simulation model was then used as input to two different thermal hydraulic models of a PWR fuel pin channel to demonstrate the potential of the new dynamic moving boundary model.

DNBR is a ratio of critical heat flux (CHF) at a given location within a channel to actual heat flux at that location. A ratio greater than one indicates CHF has not been reached, a ratio equal to one indicates CHF has

been reached, while a ratio less than one indicates CHF has been exceeded.

CHF is a phenomenon that results from a sudden reduction in heat transfer capability between a two-phase coolant and a heated surface. Physically the reduction occurs because of a change in liquid-vapor flow patterns at the heated surface. At low void fractions typical of PWR operating conditions the heated surface can transition from a wetted surface with nucleate boiling to a vapor-blanketed surface. This results in a clad surface temperature excursion called Departure from Nucleate Boiling (DNB) (Todreas & Kazimi 1990). The transition can be caused by an increase in heat flux or a reduction in cooling.

CHF is one of two Safety Analysis Fuel Design Limits (SAFDL) that limit maximum power output on a given nuclear reactor. MDNBR is not allowed to go below a minimum value for a given nuclear power plant in any part of the core during any transient. Correlations that are chosen to predict DNBR directly affect magnitude of the calculated margin of safety between maximum heat flux and minimum critical heat flux. If a new correlation is used that more accurately simulates actual channel conditions and predicts a higher value of MDNBR, then the reactor can be

operated at higher powers without reducing actual thermal margin.

Current major thermal-hydraulic codes use a quasi-steady state fixed boundary formulation. This thesis analyses whether a new dynamic moving boundary thermal hydraulic fuel pin model results in a gain in thermal margin during transient conditions.

METHOD

This study of relationships between MDNBR and position of MDNBR versus time was conducted by using five different computer models.

1) CEPAC (Combustion Engineering Plant Analysis Code)

2) LASAN (Los Alamos System ANalysis)

3) CEPAC-L: CEPAC linked with LASAN

4) COBRA: a quasi-steady state fixed boundary thermal hydraulic analysis code

5) FUELPIN: a new thermal hydraulic model which uses a dynamic moving boundary approach.

CEPAC is a general code created by Combustion Engineering specifically for plant transient analysis of system-80 PWRs, similar to ones used at Palo Verde Nuclear Generation station. CEPAC, while an accurate representation of a PWR, does not have a very sophisticated fuel pin model or allow users to significantly change the input or output of the program.

LASAN is a general purpose code developed at Los Alamos National Laboratory to provide a method of solving large systems of non-linear ordinary differential equations. LASAN was used to control input, output and time but not for computations in this application.

CEPAC-L is a non-proprietary version of CEPAC written to link with LASAN in order to give users much more flexibility and control over input and output, and to allow new models to be incorporated. CEPAC-L and CEPAC use identical calculation methods with the exception of some proprietary control system models. CEPAC-L was placed on VAX at the University of Arizona and compared to output of CEPAC for this thesis.

FUELPIN is a dynamic moving boundary model of a fuel pin created at the University of Arizona (Han 1993). It was linked to CEPAC-L to get MDNBR and position of MDNBR outputs versus time for a complete loss of primary coolant flow transient. No calculations or variables from FUELPIN were fed back into CEPAC-L.

Finally, output of FUELPIN was compared to output of COBRA, a quasi-steady state fixed boundary thermal hydraulics computer code. Identical inputs were given to COBRA and FUELPIN from CEPAC-L.

Specifically, relationships between MDNBR, position of MDNBR and time were analyzed by comparing:

1) output of COBRA with inputs from CEPAC-L and

2) output of FUELPIN with inputs from CEPAC-L

In both cases CEPAC-L used LASAN to control input, output and time. CEPAC was used as a benchmark for analyzing the CEPAC-L code simulation of Palo Verde.

Palo Verde Nuclear Power Plant

Palo Verde nuclear power plant is a 3800 MW System-80 pressurized water reactor built by Combustion Engineering. Figure 1 is a basic diagram of Palo Verde's nuclear steam supply system (ANPP 1984). Table 1 summarizes basic plant data (ANPP 1984).

Table 1. Palo Verde Nuclear Power Plant Data

Design Thermal Power (MWt)	3817
Number of Loops	2
Number of Steam Generators per loop	1
Number of Pumps per loop	2
Operating Pressure (psig)	2250
Operating Cold Leg Temp, full power (F)	564.5
Operating Hot Leg Temp, full power (F)	621.2
Coolant Flow Rate (lbm/sec)	45556
Steam Pressure, full power (psig)	1070
Steam Flow, full power (lbm/sec)	2386

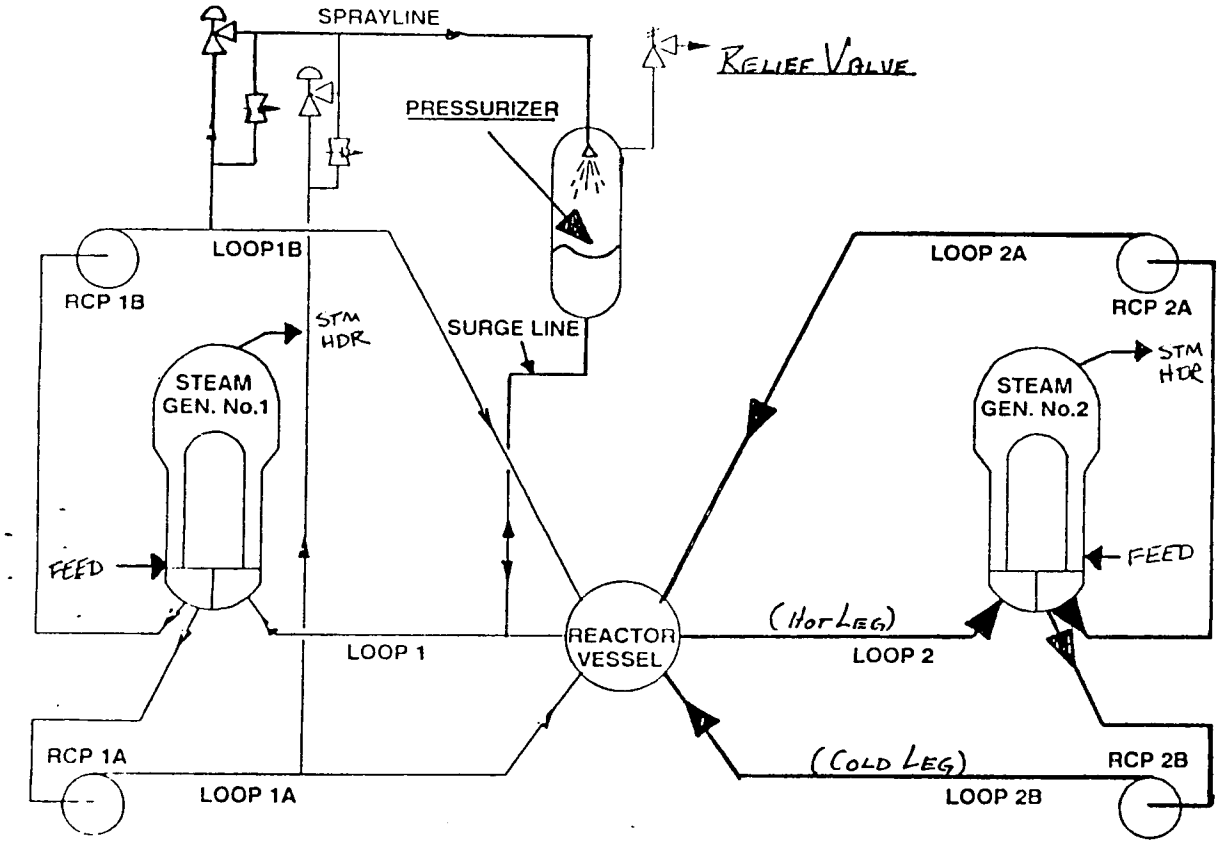

Figure 1. Palo Verde System-80 PWR

CEPAC Computer Code Description

CEPAC was developed by Combustion Engineering (C-E) as a nuclear steam supply system transient simulation code based on C-E's digital simulation code CESEC. The plant database is a system-80 PWR similar to the plant at Palo Verde Nuclear Generating Station. Users can select transient type, control visual display of output on the monitor and determine what data is saved for graphs.

CEPAC was designed to be a best estimate thermal-hydraulic tool. It was not reviewed according to quality assurance procedures, and was not intended to be used for licensing analysis. However, results were bench marked against other full scope simulator codes (CEPAC 1993).

CEPAC is an executable code whose model can not be changed since it is proprietary information for Combustion Engineering and its clients. In addition, its input and output features are limited.

LASAN Computer Code Description

LASAN is a general purpose code developed to provide a method of solving large systems of nonlinear ordinary differential equations. The modeled system may be represented by a set of subroutines called modules. LASAN is an executive code which has steady state, transient, and frequency response solution capabilities. The code is

written in FORTRAN 77 programming language and is in use on University of Arizona's VAX computer (Secker 1979).

CEPAC-L was written in LASAN modules in order to take advantage of flexible input and output features LASAN provided. The full computational powers of LASAN were not used in CEPAC-L or FUELPIN.

CEPAC-L Computer Code

CEPAC-L was developed by Palo Verde engineers as a non-proprietary version of CEPAC. Most of CEPAC-L is identical to CEPAC with the exception of two control system models and the fact that CEPAC-L is written in LASAN modules. LASAN controls input, output and time which gives users more flexibility. In addition, programmers have the ability to change, add or delete modules of code.

CEPAC-L uses various subroutines to model key nuclear steam supply system components such as reactor vessel and core, steam generators, coolant loops, pressurizer and reactor coolant pumps. These systems model pressurizer sprays, heaters and safety valves, safety injection pumps, charging and letdown systems, and reactor regulating and shutdown rods.

The secondary system models key components out to the turbine throttle valves. Steam generators receive feed water from main and auxiliary feed systems. Main steam

lines contain atmospheric dump, main steam safety, main steam isolation, and steam bypass valves (CEPAC-L 1993).

Output from CEPAC-L was used as input to both COBRA and FUELPIN. For COBRA, CEPAC-L output was manually inserted into COBRA's input file. FUELPIN and CEPAC-L were linked together through LASAN. There was no feedback allowed to CEPAC-L from calculations done in FUELPIN, in order to do a completely independent comparison between COBRA and FUELPIN.

A graphical comparison between CEPAC-L and CEPAC outputs for steady state operation and a complete loss of primary coolant flow casualty are given in RESULTS. Module causality diagrams for CEPAC-L are in Appendix A.

Mass and Energy Calculations.

Pressurizer, steam generator and upper head modules are divided into regions that contain different phases of coolant that exist or could exist in each component. The pressurizer and steam generator modules contain three regions each, while the upper head module contains two regions.

The pressurizer was divided into a vapor region, a subcooled liquid region for inflow from a surge line and a saturated liquid region, between the other two regions, surrounding the pressurizer heaters. The steam generators were divided into downcomer, evaporator riser and steam

dome regions. The upper head is divided into liquid and vapor regions for severe transients which draw a bubble in the reactor vessel.

Volume of each region is dynamically calculated in time based on total mass and energy associated with the region. Modules conserve mass and energy in each region by using the following relationships:

$$\frac{dM}{dt} = \sum W_{in} - \sum W_{out}$$

$$\frac{dU}{dt} = \sum (Wh)_{in} - \sum (Wh)_{out} + \sum \dot{Q}_{in} - \sum \dot{Q}_{out}$$

M = total mass

U = total internal energy

W = mass flow rate

h = specific entalpies

$\dot{Q}$ = heat transfer rate

t = time

These equations are integrated over time to determine new component pressures by an iterative solution of

$$M_f v_f(p) + M_g v_g(p) = V$$

$$M_f + M_g = M$$

$$M_f u_f(p) + M_g u_g(p) = U$$

M_f, M_g = liquid and steam masses

v_f, v_g = liquid and steam specific volumes

u_f, u_g = liquid and steam internal energies

P = pressure

V = total volume

The reactor coolant system module contains eight nodes for each of two reactor coolant loops. A mass and energy balance is performed on each of these nodes (CEPAC-L 1993):

$$\frac{dM_i}{dt} = W_{in} - W_{out} + W_{term}$$

W_{in}, W_{out} = mass flow rate in and out of node

M_i = mass of node

W_{term} = mass flow rate in and out of node due to leaks and crossflow

In general for a fixed volume node the energy balance is:

$$\frac{d(Mu)}{dt} = W_{in}h_{in} - W_{out}h_{out} + Q_{term}$$

Q_{term} = heat flow rate in and out of node due to leaks and crossflow

Expanding the left hand side:

$$\frac{d(Mu)}{dt} = \frac{d}{dt}(Mh - PV) = M\frac{dh}{dt} + h\frac{dM}{dt} - V\frac{dP}{dt}$$

The energy equation for a single node becomes:

$$M_i\frac{dh_i}{dt} = W_{in}h_{in} - W_{out}h_i + Q_{term} - h_i\frac{dM_i}{dt} + V\frac{dP}{dt}$$

h_i = node average enthalpy

In this equation outlet enthalpy is assumed to be the node average enthalpy. This equation can be simplified further if Pressure is assumed to be constant throughout the node for the current time step.

$$M_i\frac{dh_i}{dt} = W_{in}h_{in} - W_{out}h_i + Q_{term} - h_i\frac{dM_i}{dt}$$

A mass balance on total fluid in the reactor coolant system is calculated each time step to determine a new pressurizer surge line flow for the next time step. The

result is used by the pressurizer model in the next time step to calculate a new system pressure.

Core fuel temperatures are calculated by a core energy balance which divides the core into one section for each steam generator. A fuel temperature is calculated for each section. Core fuel and cladding mass are lumped together and heat transfer is defined by a single constant value (CEPAC-L 1993).

$$\frac{dT_f}{dt} = \frac{1}{M_{core}CP_{core}}\left[\frac{Q_{core}}{2} - HFRCS\frac{ACORE}{2}(T_f - T_c)\right]$$

where:

T_f = fuel temperature

T_c = coolant temperature

M_{core} = core mass (fuel + cladding)

CP_{core} = core specific heat

Q_{core} = core power

HFRCS = fuel to coolant heat transfer coefficient

A_{core} = heat transfer area of core

Heat Transfer Calculations.

Heat transfer between regions and nodes, and between components within modules is calculated by variations of a basic heat transfer equation (Incropera et. al. 1981):

$$\dot{Q} = h\ A\ \Delta T$$

$\dot{Q}$ = heat transfer rate

h = heat transfer coefficient

A = heat transfer area

ΔT = temperature gradient

Primary to secondary heat transfer in the steam generator is determined by this general relation:

$$\dot{Q}_{p\text{-}s} = U\ A\ (T_{pri} - T_{sec})$$

$\dot{Q}_{p\text{-}s}$ = heat transfer from primary to secondary

U = overall heat transfer coefficient

T_{pri} = hot leg primary coolant temperature

T_{sec} = secondary feed / steam temperature

where:

$$U = \frac{1}{\frac{1}{h_{pri}} + R_{tubes} + \frac{1}{h_{sec}}}$$

h_{pri} = primary fluid heat transfer coefficient

h_{sec} = secondary fluid heat transfer coefficient

R_{tubes} = thermal resistance of SG tubes

The primary heat transfer coefficient is calculated by Dittus-Boelter's correlation (Todreas et. al. 1990). The secondary heat transfer coefficient is calculated by the modified-Rohsenow heat transfer correlation for pool boiling (Rohsenow et. al. 1963). All other heat transfer coefficients are constants based on materials concerned such as pressurizer and reactor vessel materials to each other.

Flow Rate Calculations.

Flow rates are computed using various formulations, depending on type of flow. Steam flow from riser to steam dome in the steam generator as well as steam rise velocity in the pressurizer is calculated using Wilson's bubble rise correlation.

Liquid flow from downcomer to riser is calculated with a quasi-steady state momentum balance (CEPAC-L 1993):

$$W_{32} = F_{32}\sqrt{\rho_3 H_3 - \rho_2 H_2}$$

W_{32} = mass flow rate from downcomer to riser

F_{32} = correlating coefficient

ρ_2, ρ_3 = densities of downcomer and riser regions

H_2, H_3 = heights of the downcomer and riser

Primary coolant flow is calculated using a solution of a one-dimensional momentum equation for each pump loop. The reactor coolant system is divided into 28 nodes. Forces acting on the fluid volume consist of:

1) gravitational forces due to density and elevation changes around the loop,
2) viscous forces due to wall friction and geometric expansions and contractions of the piping, and
3) forces due to reactor coolant pumps

Therefore (CEPAC-L 1993):

$$\frac{dW}{dt} = \frac{g\sum_{i=1}^{n}(\rho_i z_i) - \sum_{i=1}^{n} W_i^2\left(\frac{f_i R_{fric,i} + R_{geo,i}}{\rho_{is}}\right) + \Delta P_{pump}}{\sum_{i=1}^{n}\left(\frac{L_i}{A_i}\right)}$$

W = mass flow rate at the pump

W_i = mass flow rate of ith node

ρ_i = average fluid density of ith node

ρ_{is} = single phase fluid density of ith node

z_i = elevation difference across the ith node

f_i = Darcy friction factor for the ith node

L_i = effective flow path length for the ith node

A_i = effective cross sectional flow area of ith node

where:

$$R_{fric,i} = \frac{\frac{L_i}{D_{e,i}}}{2A_i^2}$$

$$R_{geo,i} = \frac{K_{g,i}}{2A_i^2}$$

$D_{e,i}$ = effective diameter of ith node

$K_{g,i}$ = dimensionless geom. proportionality const

Flow through the reactor coolant system in natural circulation mode is also calculated as well as resistance to natural circulation flow from the reactor coolant pumps.

COBRA Computer Code

COBRA IV PC code is a personal computer version of the COBRA-IV computer program developed at Pacific Northwest Laboratory by Battelle-Northwest. It is a thermal hydraulic modeling code that uses a subchannel analysis approach to determine enthalpy and flow distributions in rod bundles for steady-state conditions.

The basic idea is to divide the reactor core into computational cells. Balance laws of mass, energy and momentum for the fluid are written for each cell where independent variables of enthalpy, pressure and velocity are appropriate averages. Cells may have fuel rods or other solid materials which act as sources or sinks of heat

and momentum to the fluid. Transient thermal response of fuel or solids is included and is interfaced with the hydraulics through heat transfer coefficients. Use of the computational cell concept allows subchannel analysis, core analysis and general flow field analysis to be considered in a unified approach (Webb).

Inputs to COBRA are system pressure, core inlet temperature, core inlet mass flux, and core average heat flux. Channel layout, channel dimensions, fuel pin materials and axial heat flux distribution are inputs as well. Temperature profiles, enthalpies, heat flux, CHF and DNBR at various channel axial positions are all outputs from COBRA.

Correlations Used.

COBRA uses several different heat transfer correlations to determine channel parameters. In general heat flux in forced convection heat transfer is determined by using the general formula (Incropera 1981):

$$q'' = h\ (T_{wall} - T_{bulk})$$

q" = heat flux
h = heat transfer coefficient
T_{wall} = clad wall temperature
T_{bulk} = bulk moderator temperature

To determine heat transfer coefficients for pre-CHF single phase forced convection COBRA uses Dittus-Boelter's correlation (Todreas et. al. 1990):

$$h = \frac{k}{D_H} 0.023 \mathrm{Re}^{0.8} \mathrm{Pr}^{0.4}$$

$$\mathrm{Re} = \frac{\rho v D_e}{\mu}$$

$$\mathrm{Pr} = \frac{\mu c_p}{k}$$

k = thermal conductivity of the coolant

D_H = hydraulic diameter of the channel

Re = Reynolds number

Pr = Prandtl number

ρ = fluid density

v = fluid velocity

D_e = channel equivalent diameter

μ = fluid viscosity

c_p = fluid heat capacity

Table 2 lists various correlations used by COBRA to calculate heat transfer coefficients.

Table 2. Correlations used by COBRA

Subcooled liquid region	Dittus-Boelter
Subcooled boiling region	Thom correlation
Nucleate boiling region	Thom correlation
Saturated boiling region (pre-CHF)	Schrock and Grossman correlation
Transition boiling (post-CHF)	McDonough, Milich and King correlation
Film boiling	Groeneveld correlation
Critical Heat Flux	W - 3 correlation

The W-3 correlation was used to predict CHF in all cases throughout channel length. This correlation was developed for axially uniform heat flux, with a correcting factor for nonuniform flux distribution. For a channel with axially uniform heat flux in British units (Todreas et. al. 1990):

$$
\begin{aligned}
q''_{cr}/10^6 = {} & \left\{(2.022 - 0.0004302p) + (0.1722 - 0.0000984p)\exp[(18.177 - 0.004129p)x_e]\right\} \\
& \times\left[(0.1484 - 1.596x_e + 0.1729x_e|x_e|)G/10^6 + 1.037\right] \\
& \times(1.157 - 0.869x_e)[0.2664 + 0.8357\exp(-3.151D_h)] \\
& \times[0.8258 + 0.000794(h_f - h_{in})]
\end{aligned}
$$

q''_{cr} = critical heat flux

p = pressure

x_e = local thermodynamic quality

G = mass flux

h_f = saturated liquid entalpy

h_{in} = inlet enthalpy

The axially non-uniform heat flux is obtained by applying a correction factor to the uniform critical heat flux (Tong 1972):

$$q''_{cr,n} = q''_{cr}/F$$

$q''_{cr,n}$ = non-uniform critical heat flux

F = Tong correction factor

Dynamic Moving Boundary Fuel Pin Model

FUELPIN was developed to accommodate the moving boundary thermal hydraulic model. The model is suitable for both PWR and BWR fuel rods consisting of UO-2 pellets enclosed in hollow zircaloy-2 tubes. The model addresses thermal and physical properties of fuel as well as gap conductance between fuel and zircaloy-2 cladding. Physical properties of fuel and cladding are treated as functions of temperature.

Fluid Flow.

Figure 2 illustrates flow regimes through a vertical channel. As fluid travels up the channel energy is continuously added causing rising moderator and fuel temperatures. Rising wall temperatures lead to subcooled boiling, nucleate boiling, saturated boiling and finally when critical heat flux is reached film boiling. Eventually, if the transient continues heat transfer will be to saturated then superheated vapor.

Positions within the channel where these conditions occur vary with time during the transient. The dynamic moving boundary model calculates the positions of these boundaries and uses them to more accurately predict channel parameters. The moving axial boundaries in this model are axial positions of:

1) subcooled nucleate boiling
2) saturated liquid
3) departure from nucleate boiling
4) re-wetting of heat transfer surface
5) superheated vapor

There are two fixed axial positions at inlet and outlet of the channel. Figure 3 illustrates the positions of the moving boundaries along a vertical channel. Table 3 lists the various correlations used by the moving boundary model to determine heat transfer coefficients (Han 1993).

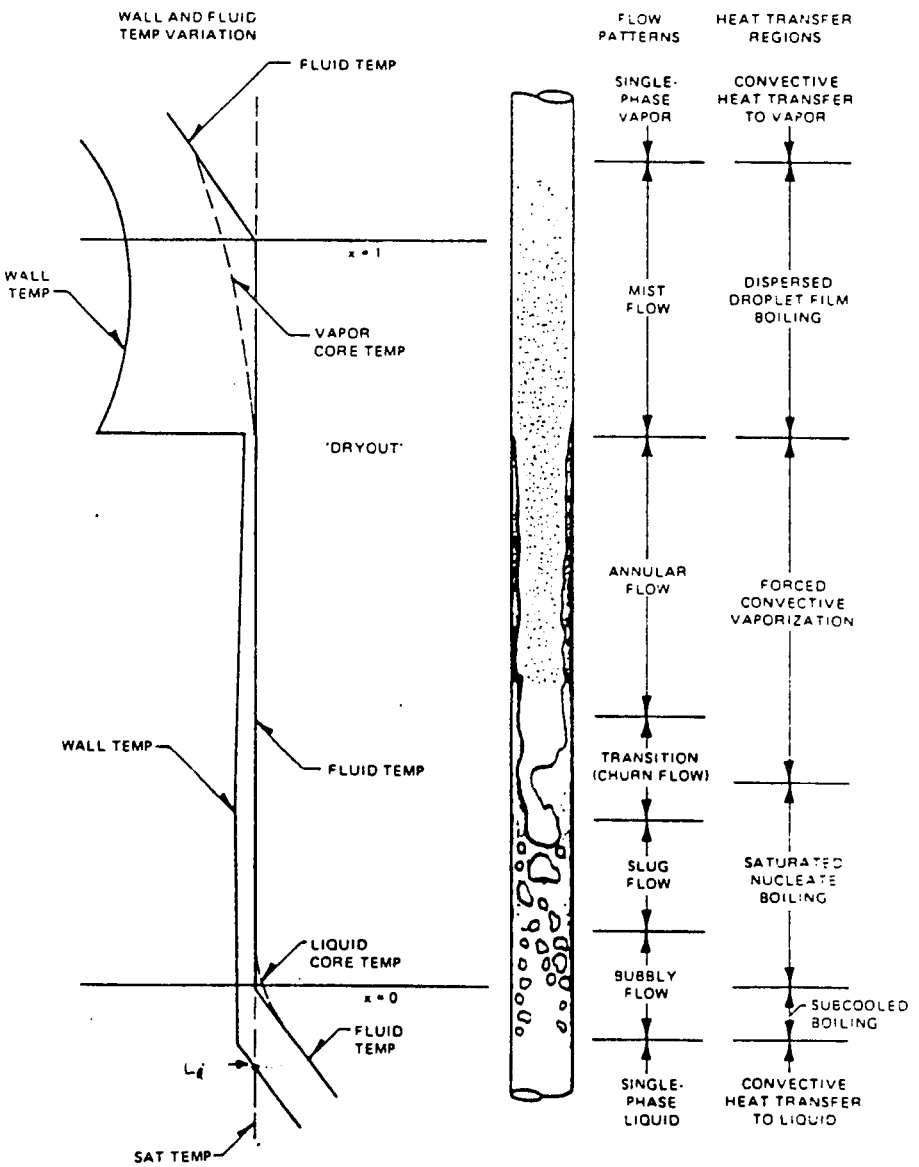

Figure 2. Single Channel Flow Regimes

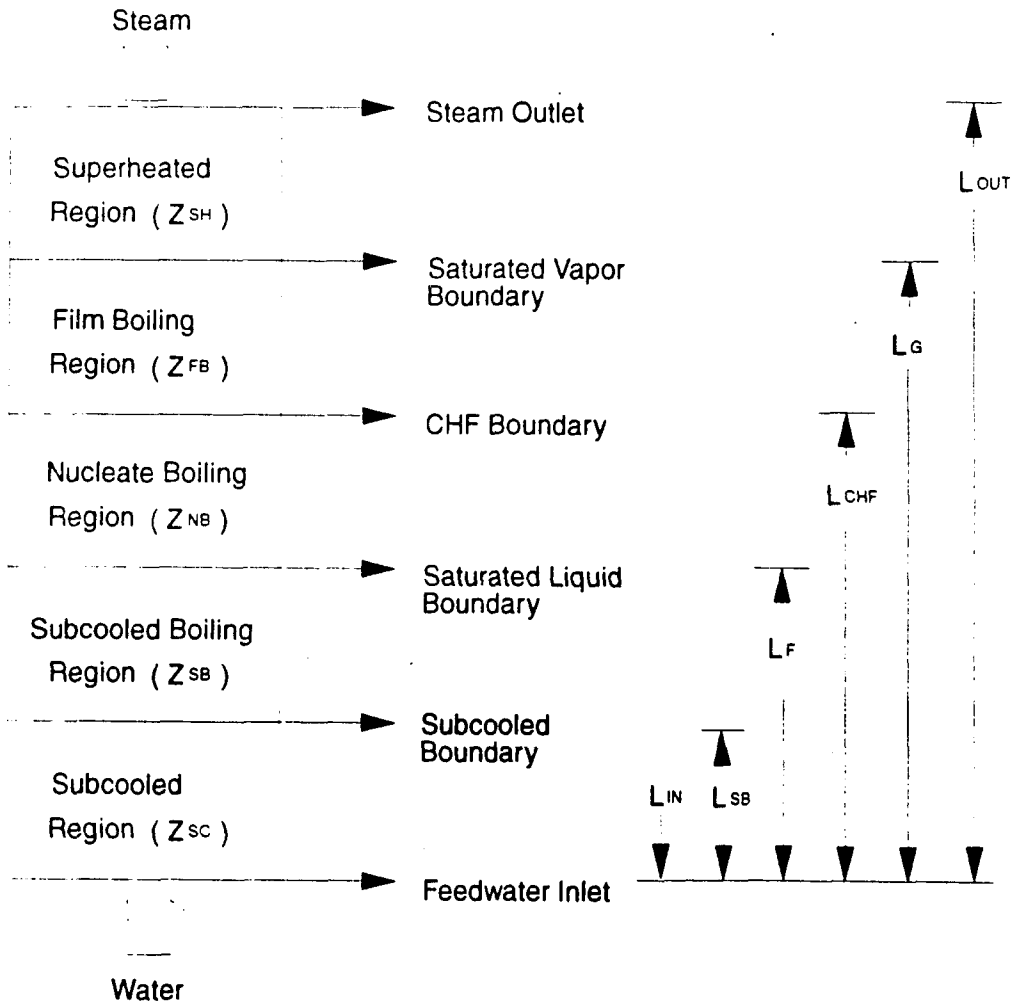

Figure 3. Moving Boundary Model in a Boiling Channel

Table 3. Correlations used by FUELPIN

Subcooled liquid region	Dittus-Boelter
Subcooled boiling region	Chen correlation
Nucleate boiling region (pre-CHF)	Chen correlation
Film boiling (post-CHF)	Bishop correlation
Superheat region	Colburn correlation
Critical heat flux	W - 3 correlation

Some of the correlations used by FUELPIN are not identical to those used by COBRA. However, all have been proven to be valid for their corresponding channel conditions. In addition, the only ones used in this comparison are for the subcooled liquid region. The Dittus-Boelter correlation is used by both COBRA and FUELPIN in this region, and both codes use the W-3 correlation for critical heat flux.

FUELPIN uses a four equation model to calculate core thermal hydraulic parameters. Balances are performed for each node on:

1) Liquid mass
2) Vapor mass
3) Mixture energy
4) Mixture momentum

Heat Transfer.

In general for a homogeneous system heat flux can be calculated by solving the basic heat transfer equation for a heat generating cylindrical pin.

$$A\frac{d}{dt}(\rho h) = Aq''' - P_h q''$$

A = cross sectional area

P_h = hydraulic perimeter

ρ = density

h = enthalpy

q'' = heat flux

q''' = heat generation rate

where:

$$q'' = U\,(\,T_f - T_m\,)$$

U = overall heat transfer coefficient

T_f = centerline fuel temperature

T_m = bulk moderator temperature

solving for heat flux:

$$q'' = \frac{A}{P_h} q''' - \frac{A}{P_h}\frac{d}{dt}(\rho h)$$

COBRA uses this method to calculate a local heat flux however, since it assumes steady state the time dependent term is neglected.

The time dependent term is not neglected in the FUELPIN model. The transient and steady-state temperature distributions in the fuel pin are obtained by solving the classical Fourier heat conduction equation (Lahey et. al. 1977).

$$\frac{d\rho h(r,z,t)}{dt} = \nabla \cdot k(T) \nabla T(r,z,t) + q'''(r,z,t)$$

where:

ρ = density

h = specific enthalpy

k = conductivity

T = temperature

q''' = volumetric heat generation rate

r = radial position

z = axial position

t = time

In cylindrical geometry the heat conduction equation can be written as

$$\frac{d}{dt}[\rho h(r, z, t)] = \frac{1}{r}\frac{\partial}{\partial r}\left(k(T)\, r \frac{\partial T(r, z, t)}{\partial r}\Big|_{z}\right) + \frac{\partial}{\partial z}\left(k(T)\, \frac{\partial T(r, z, t)}{\partial z}\Big|_{r}\right) + q'''(r, z, t)$$

In some fuel pin solutions where fixed axial nodes are used the axial z-dependence effects are neglected. In the moving boundary model including the axial effects provides a measure of numerical stability when the axial boundaries are near each other. To solve for the transient temperature distribution the cylindrical geometry equation is integrated in both the r and z directions over the fuel pin geometry. Figure 4 shows a general spatial grid for transient conduction analysis (Lahey et. al. 1977). FUELPIN uses three radial fuel zones and one radial zone for the cladding.

By integrating the cylindrical heat conduction equation over each volume node:

$$\int_{L_i}^{L_{i+1}} 2\pi \int_{r_{i-1}}^{r_i} r \frac{d}{dt}(\rho h)\, dr dz = \int_{L_i}^{L_{i+1}} 2\pi \int_{r_{i-1}}^{r_i} \frac{\partial}{\partial r}\left(kr \frac{\partial T}{\partial r}\Big|_{z}\right) dr dz + \int_{L_i}^{L_{i+1}} 2\pi \int_{r_{i-1}}^{r_i} r \frac{\partial}{\partial z}\left(k \frac{\partial T}{\partial z}\Big|_{r}\right) dr dz + \int_{L_i}^{L_{i+1}} 2\pi \int_{r_{i-1}}^{r_i} r q'''(r, z, t)\, dr dz$$

L_i, L_{i+1} = axial boundaries of the node

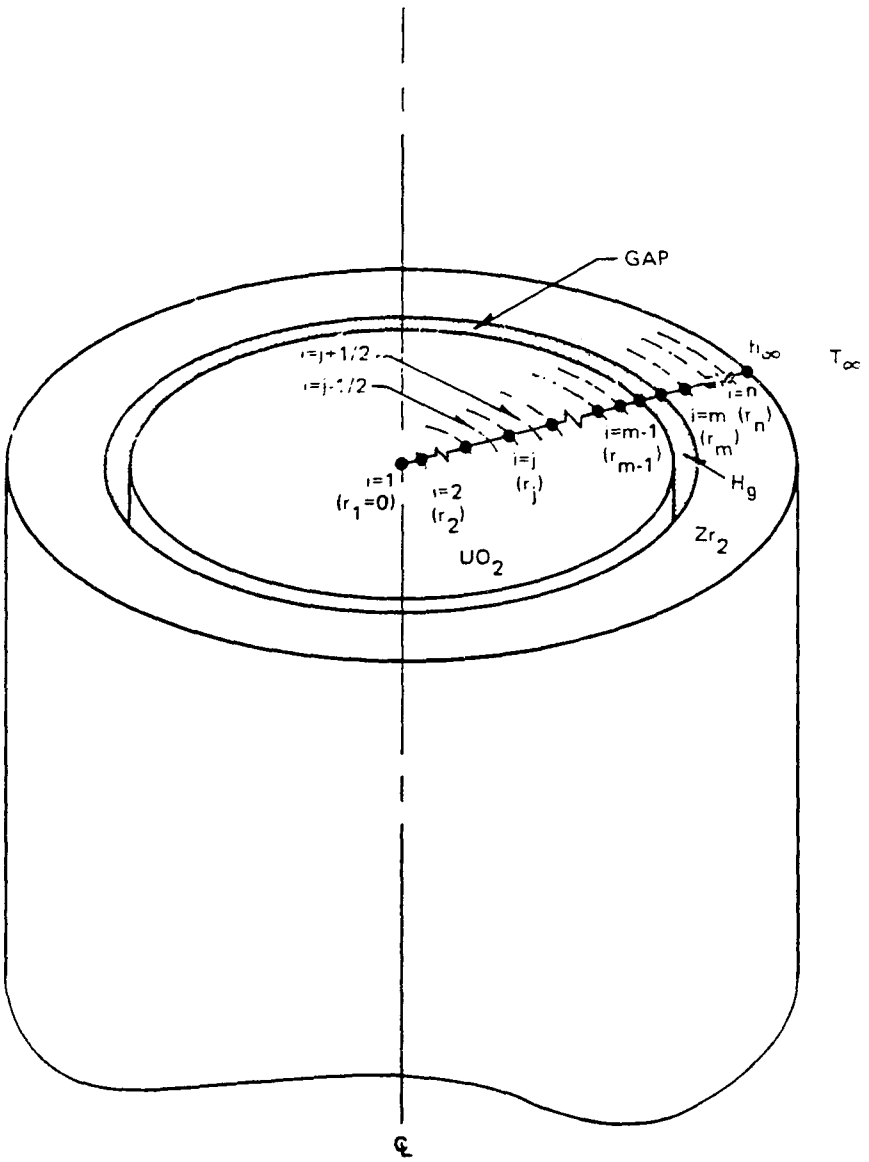

Figure 4. Spacial Grid for Transient Conduction

Performing the integration in the radial direction:

$$\int_{L_i}^{L_{i+1}} \pi\left(r_i^2 - r_{i-1}^2\right) \frac{d}{dt}(\rho h)\, dz = \int_{L_i}^{L_{i+1}} \left(2\pi r_i k \frac{\partial T}{\partial r}\Big|_{r_i} - 2\pi r_{i-1} k \frac{\partial T}{\partial r}\Big|_{r_{i-1}}\right) dz$$
$$+ \int_{L_i}^{L_{i+1}} \pi\left(r_i^2 - r_{i-1}^2\right) \frac{\partial}{\partial z}\left(k \frac{\partial T}{\partial z}\right) dz$$
$$+ \int_{L_i}^{L_{i+1}} \pi\left(r_i^2 - r_{i-1}^2\right) q'''(z, t)\, dt$$

This equation can be integrated in the z-direction, however, since L is a function of time Leibnitz rule of integration must be applied to evaluate the left-hand side. Leibnitz rule is:

$$\int_{L_i(t)}^{L_{i+1}(t)} \frac{d}{dt} f(z, t)\, dz = \frac{d}{dt} \int_{L_i(t)}^{L_{i+1}(t)} f(z, t)\, dz$$
$$- f(L_{i+1}, t) \frac{dL_{i+1}}{dt} + f(L_i, t) \frac{dL_i}{dt}$$

In cylindrical geometry values for cross-sectional area and perimeter are given by:

$$A_i = \pi\left(r_i^2 - r_{i-1}^2\right)$$
$$P_i = 2\pi r_i$$

then the cylindrical heat conduction equation becomes:

$$\int_{L_i}^{L_{i+1}} \frac{d}{dt}[A_i \rho h(r, z, t)]dz = \left(P_i k \frac{\partial T}{\partial r}\Big|_{r_i} - P_{i-1} k \frac{\partial T}{\partial r}\Big|_{r_i-1}\right)(L_{i+1} - L_i)$$
$$+ A_i\left(k_{i+1} \frac{\partial T}{\partial z}\Big|_{L_{i+1}} - k_i \frac{\partial T}{\partial z}\Big|_{L_i}\right)$$
$$+ A_i \int_{L_i}^{L_{i+1}} q'''(z, t)\, dz$$

To solve for the transient temperature distribution this equation is finite differenced in the radial direction and evaluated numerically, subject to the following boundary conditions:

$$-k_c \frac{\partial T}{\partial r}\Big|_{r=r_{co}} = q''(z, r_{co}, t) = h_\infty [T_{co}(z, t) - T_m(z, t)]$$

$$-k_c \frac{\partial T}{\partial r}\Big|_{r=r_{ci}} = q''(z, r_{ci}, t) = h_g [T_{fn}(z, t) - T_{ci}(z, t)]$$

$$-k_f \frac{\partial T}{\partial r}\Big|_{r=r_{fn}} = q''(z, r_{fn}, t) = \frac{r_{ci}}{r_{fn}} q''(z, r_{ci}, t)$$

$$-k_f \frac{\partial T}{\partial r}\Big|_{r=r_{fi}} = q''(z, r_{fi}, t) = \frac{r_{fi+1}}{r_{fi}} q''(z, r_{fi+1}, t)$$

$$\frac{\partial T}{\partial r}\Big|_{r=0} = 0$$

where:

h_∞ = convective heat transfer coefficient

h_g = fuel-clad gap conductance

T_{co} = outer clad temperature

T_{ci} = inner clad temperature

T_m = average moderator temperature

T_{fn} = outer fuel temperature

T_{fi} = outer fuel temperature of ith node

q''_r = heat flux due to thermal radiation

In order to perform the numerical finite differencing the radial temperature distribution in the fuel is expressed as a Lagrange second order polynomial which is a function of temperatures at the radial node positions.

$$T(r, z, t) = \frac{(r - r_{fi+1})(r - r_{fi})}{(r_{fi-1} - r_{fi+1})(r_{fi-1} - r_{fi})} T_{fi-1}(z, t) + \frac{(r - r_{fi-1})(r - r_{fi+1})}{(r_{fi} - r_{fi-1})(r_{fi} - r_{fi+1})} T_{fi}(z, t) + \frac{(r - r_{fi-1})(r - r_{fi})}{(r_{fi+1} - r_{fi-1})(r_{fi+1} - r_{fi})} T_{fi+1}(z, t)$$

The gradient of T(r,z,t) with respect to r is

$$\frac{\partial}{\partial r} T(r, z, t) = \frac{(2r - r_{fi} - r_{fi+1})}{(r_{fi-1} - r_{fi+1})(r_{fi-1} - r_{fi})} T_{fi-1}(z, t)$$

$$+ \frac{(2r - r_{fi-1} - r_{fi+1})}{(r_{fi} - r_{fi-1})(r_{fi} - r_{fi+1})} T_{fi}(z, t)$$

$$+ \frac{(2r - r_{fi-1} - r_{fi})}{(r_{fi+1} - r_{fi-1})(r_{fi+1} - r_{fi})} T_{fi+1}(z, t)$$

By applying the boundary condition for r=0 (i=1) a relationship is obtained for centerline fuel temperature.

$$0 = \frac{-(r_{f1} + r_{f2})}{r_{f1} r_{f2}} T_{f0}(z, t) - \frac{r_{f2}}{r_{f1}(r_{f1} - r_{f2})} T_{f1}(z, t)$$

$$- \frac{r_{f1}}{r_{f2}(r_{f2} - r_{f1})} T_{f2}(z, t)$$

Thus, the centerline temperature is

$$T_{f0}(z, t) = \frac{r_{f2}^2 T_{f1}(z, t) - r_{f1}^2 T_{f2}(z, t)}{r_{f2}^2 - r_{f1}^2}$$

Using this method the remaining radial temperatures at a given axial position can be calculated. Once the outer clad temperature is calculated the heat transfer coefficient for clad to moderator can be determined using the appropriate correlation from table 3. Once the heat transfer coefficient and wall temperature are known the local heat flux can be determined.

Critical heat flux in FUELPIN, as well as in COBRA, is calculated using the W-3 correlation. DNBR is then easily determined once the heat flux and critical heat flux are known. This process is then repeated at all axial node positions. The position of the axial nodes can change with time as the temperature distribution changes during a transient.

RESULTS

Comparison of CEPAC-L to CEPAC

A comparison between CEPAC-L and CEPAC outputs was done in order to test the new fuel pin model using a simulation code that was as close as possible to a real reactor. This comparison proves the usefulness and accuracy of the CEPAC-L model under most conditions. Overall, it was determined that at all times during steady state and for most times and parameters during a transient CEPAC-L satisfactorily predicts Palo Verde plant parameters.

Steady State.

CEPAC-L and CEPAC outputs tracked very closely for all important plant parameters during steady state. Figure 5 shows that primary plant temperatures tracked exactly. Reactor power and flow are not shown graphically because they both remain at equal and constant levels for both CEPAC-L and CEPAC.

There were very small differences in pressurizer level and pressure during steady state between CEPAC-L and CEPAC as shown in Figures 6 and 7. Both codes predicted pressurizer level and pressure cycling within normal operating bands due to heater and spray operation for

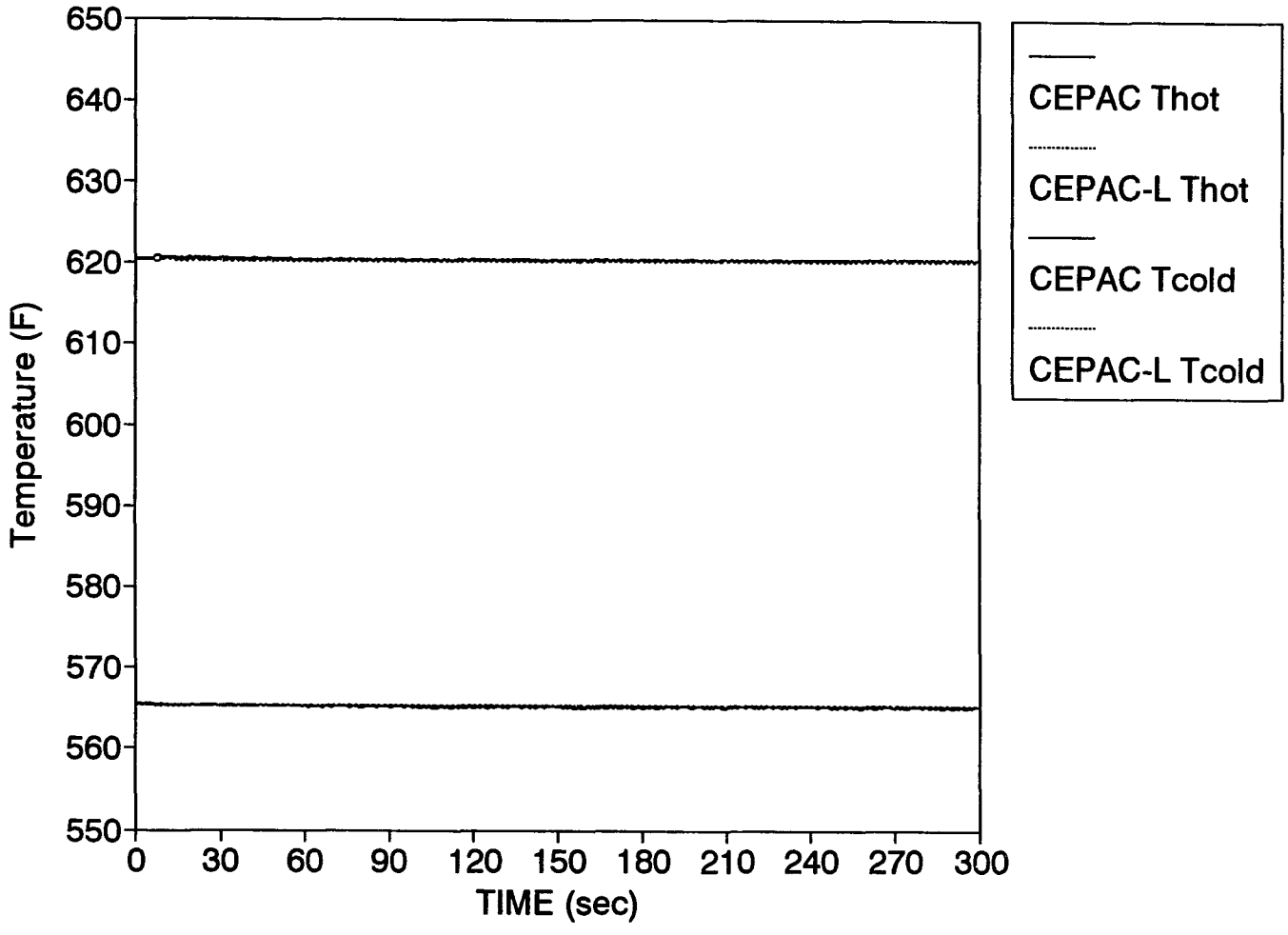

Figure 5. Loop Temperatures, Steady State

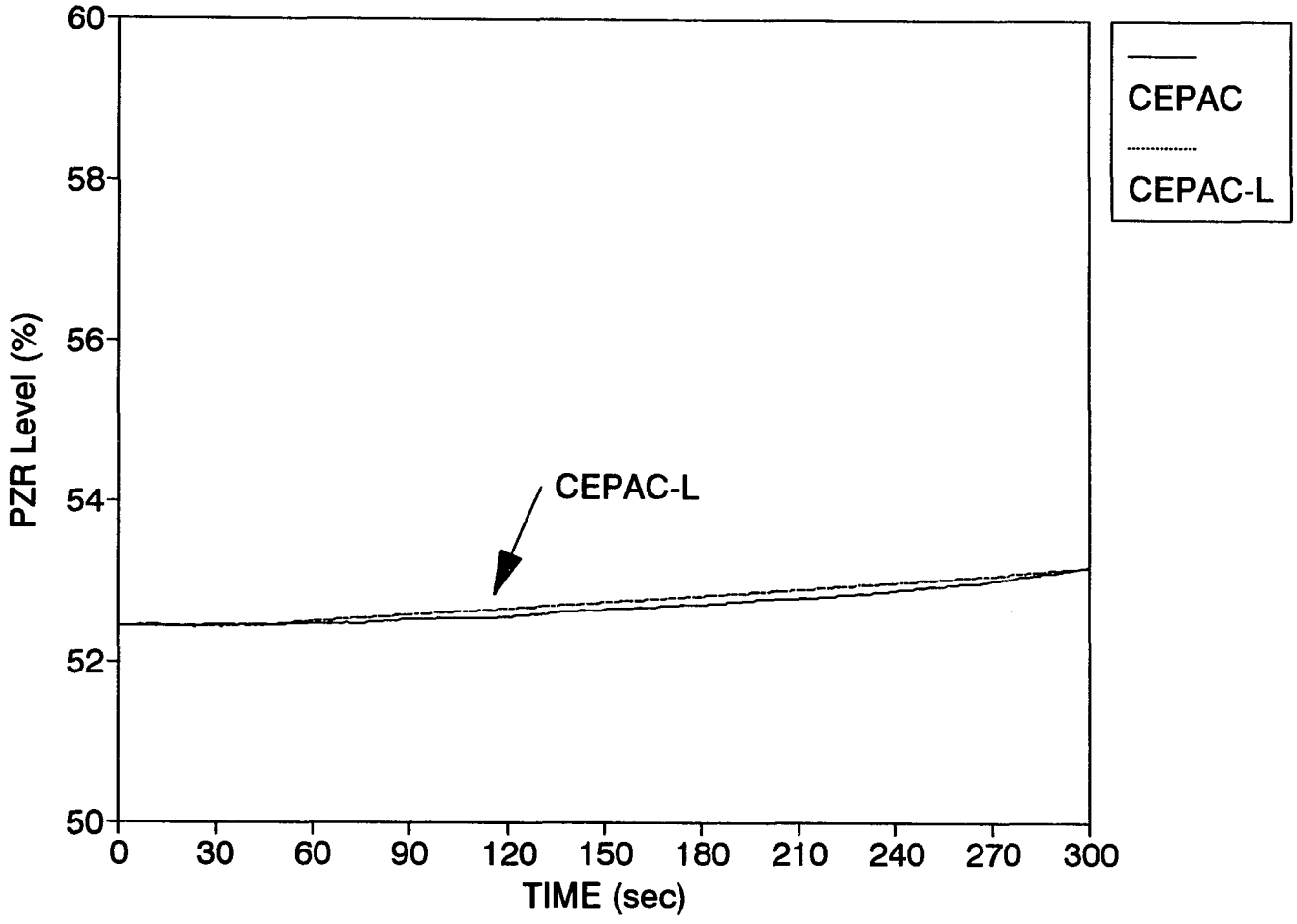

Figure 6. Pressurizer Level, Steady State

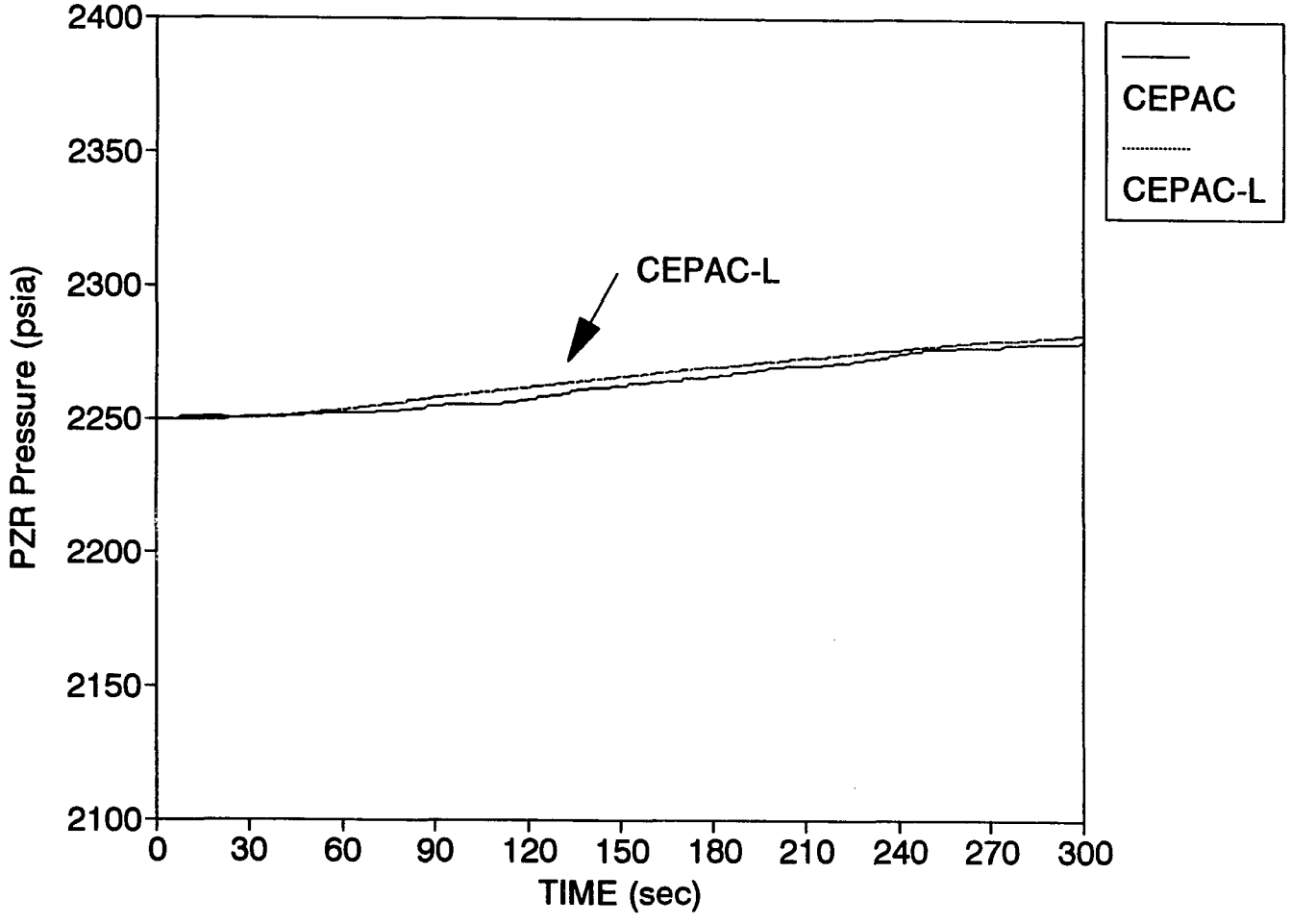

Figure 7. Pressurizer Pressure, Steady State

pressure control, and letdown and charging flows for level control.

Secondary steam and feed flows for CEPAC-L and CEPAC are shown in Figure 8. This figure illustrates the most significant difference between the two codes during steady state conditions. Feed flow in CEPAC is calculated very similar to how feed is actually controlled at Palo Verde. A control network uses steam generator water level, steam flow and actual feedwater flow as inputs to calculate a desired level setpoint, and therefore a new required feedwater flow. CEPAC-L uses a much more simplified model which adjusts feedwater flow to match steam flow, and uses a decaying value for feed flow and steam flow following a reactor trip. CEPAC predicted a more realistic output of feed flow oscillating above and below steam flow to maintain steam generator level.

Steam generator water level is very constant during steady state conditions, Figure 9, as predicted by both CEPAC and CEPAC-L. CEPAC steam generator level tended to oscillate more due to the control network used to calculate feedwater flow. CEPAC-L predicted steam generator pressure in Figure 10 to be constant but slightly higher than CEPAC due again to the differences in feedwater control models.

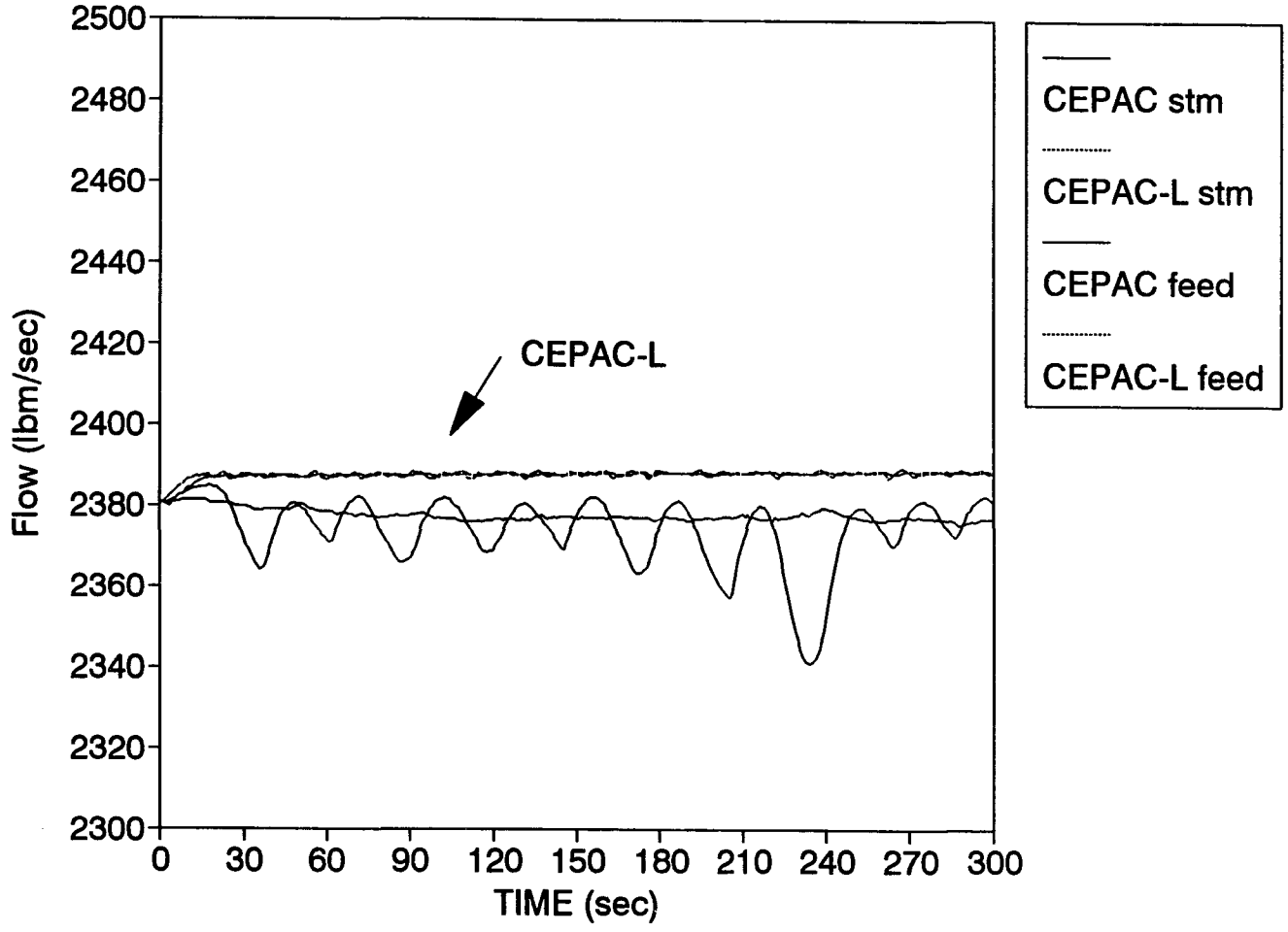

Figure 8. Steam and Feed Flows, Steady State

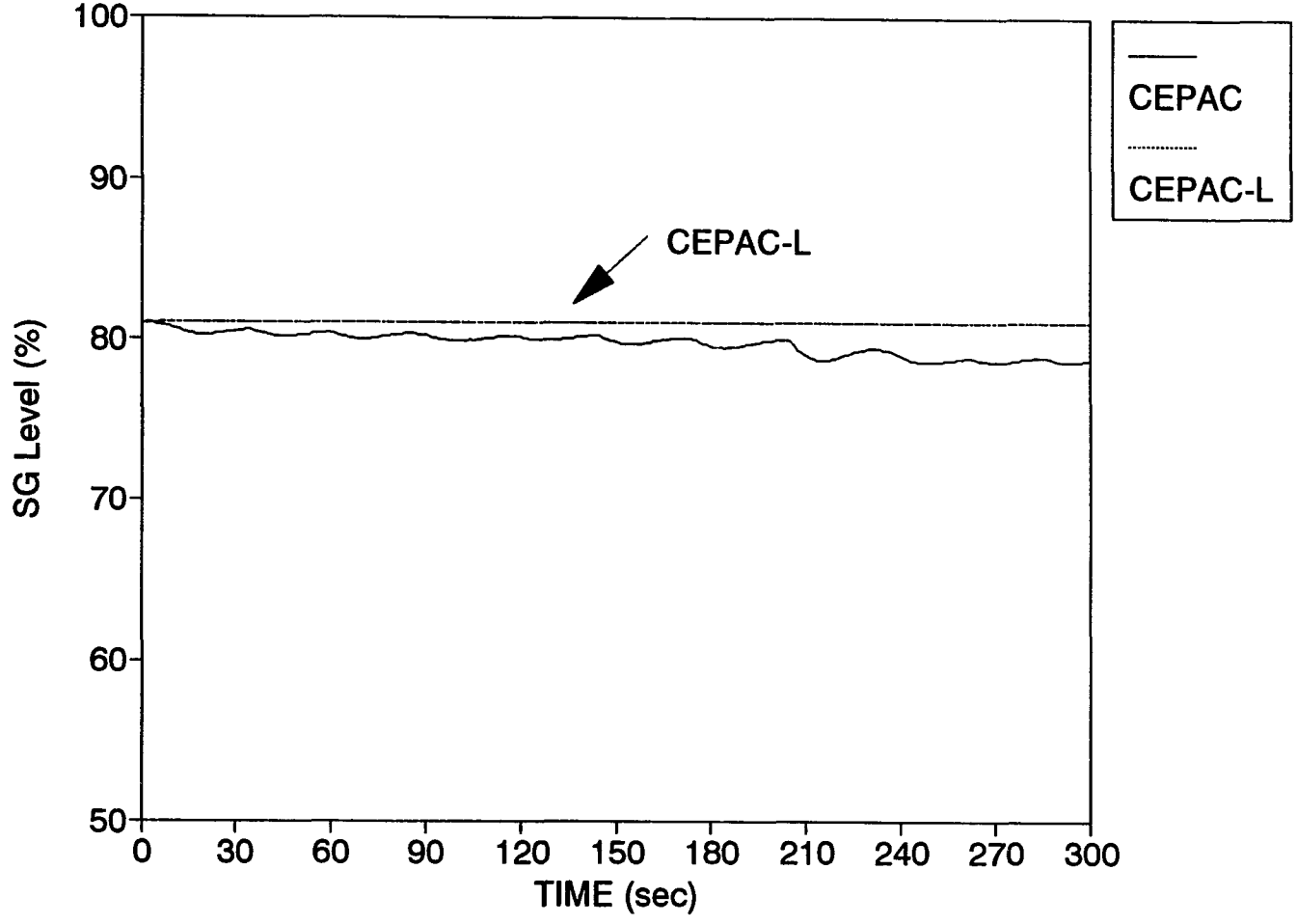

Figure 9. Steam Generator Level, Steady State

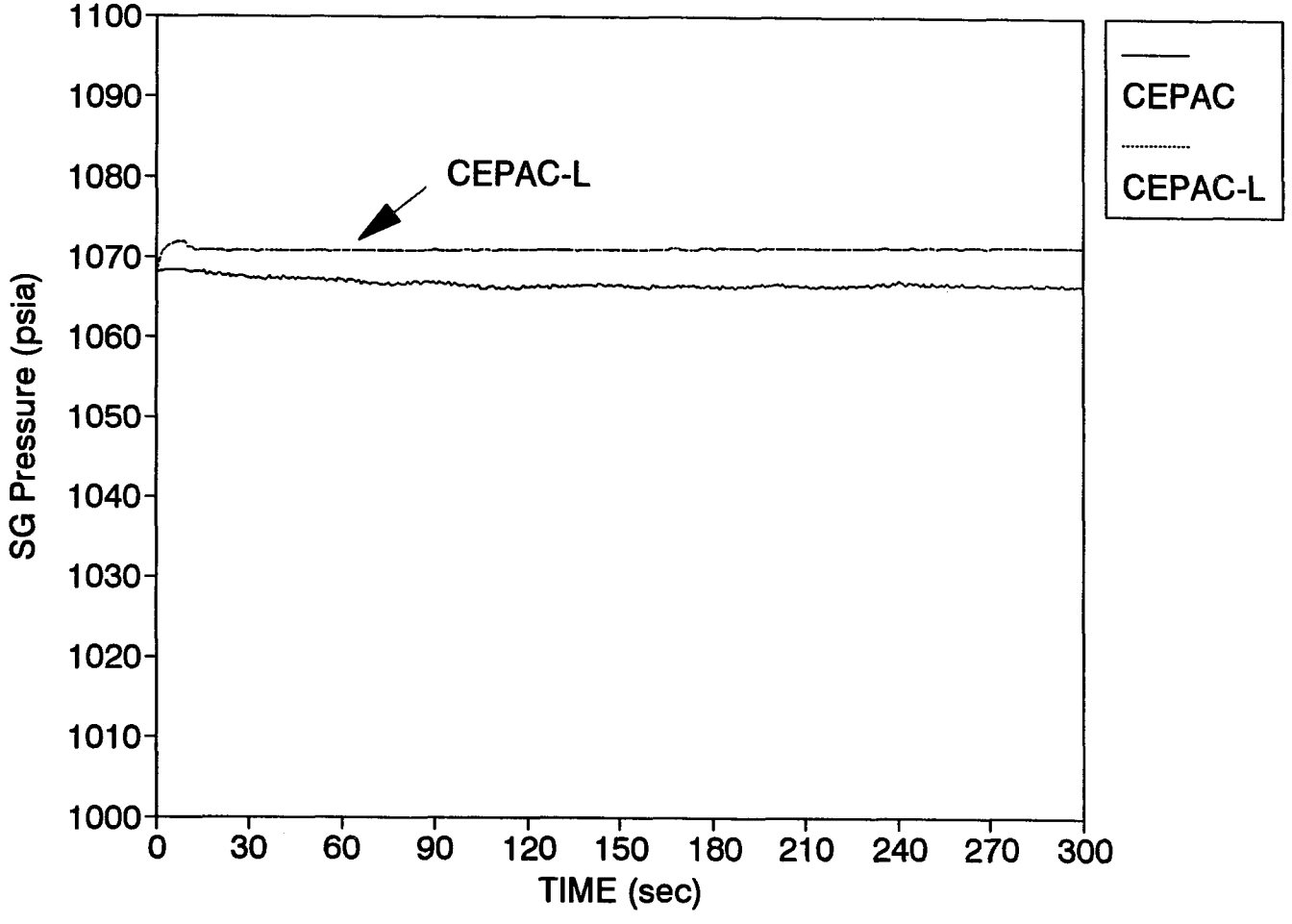

Figure 10. Steam Generator Pressure, Steady State

Loss of All Primary Coolant Flow

CEPAC-L's kinetics model calculated a reactor power transient identical to COBRA for a LOAF, as shown in Figure 11. Primary coolant flow was predicted very well by CEPAC-L following a trip of all four reactor coolant pumps and subsequent reactor scram, as expected, since both models used the same solution technique (Figure 12).

Differences exist between CEPAC-L and CEPAC in the magnitude of reactor coolant temperatures, pressurizer pressure and pressurizer level as shown in Figures 13 - 15. This was due primarily to feedback from the secondary plant during the transient after the scram.

As shown in Figure 16, CEPAC steam flow exceeds feed flow for over 30 seconds after the scram. In addition to having a more sophisticated feedwater control system model CEPAC has a more sophisticated steam bypass control system. This system mimics Palo Verde's actual steam bypass system to minimize main steam header pressure increase after a reactor scram from full power followed by an immediate turbine trip. The steam bypass control system will dump steam directly to the condenser to prevent lifting steam generator safety valves.

The CEPAC model predicted feed flow to be reduced at a faster rate than steam flow. This is accurate since the scram resulted in a rapid reduction in power which causes

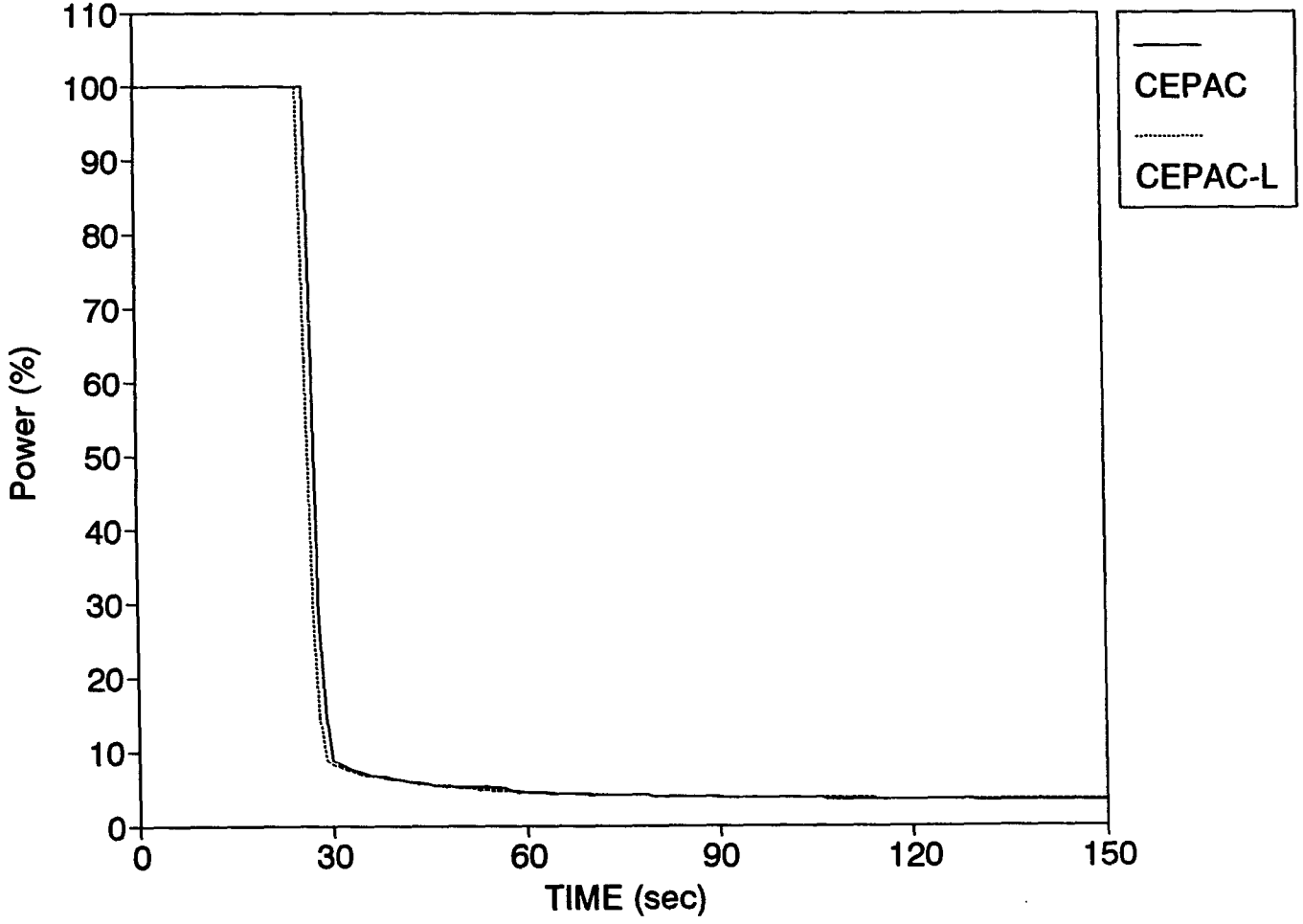

Figure 11. Reactor Power, Loss of All Flow

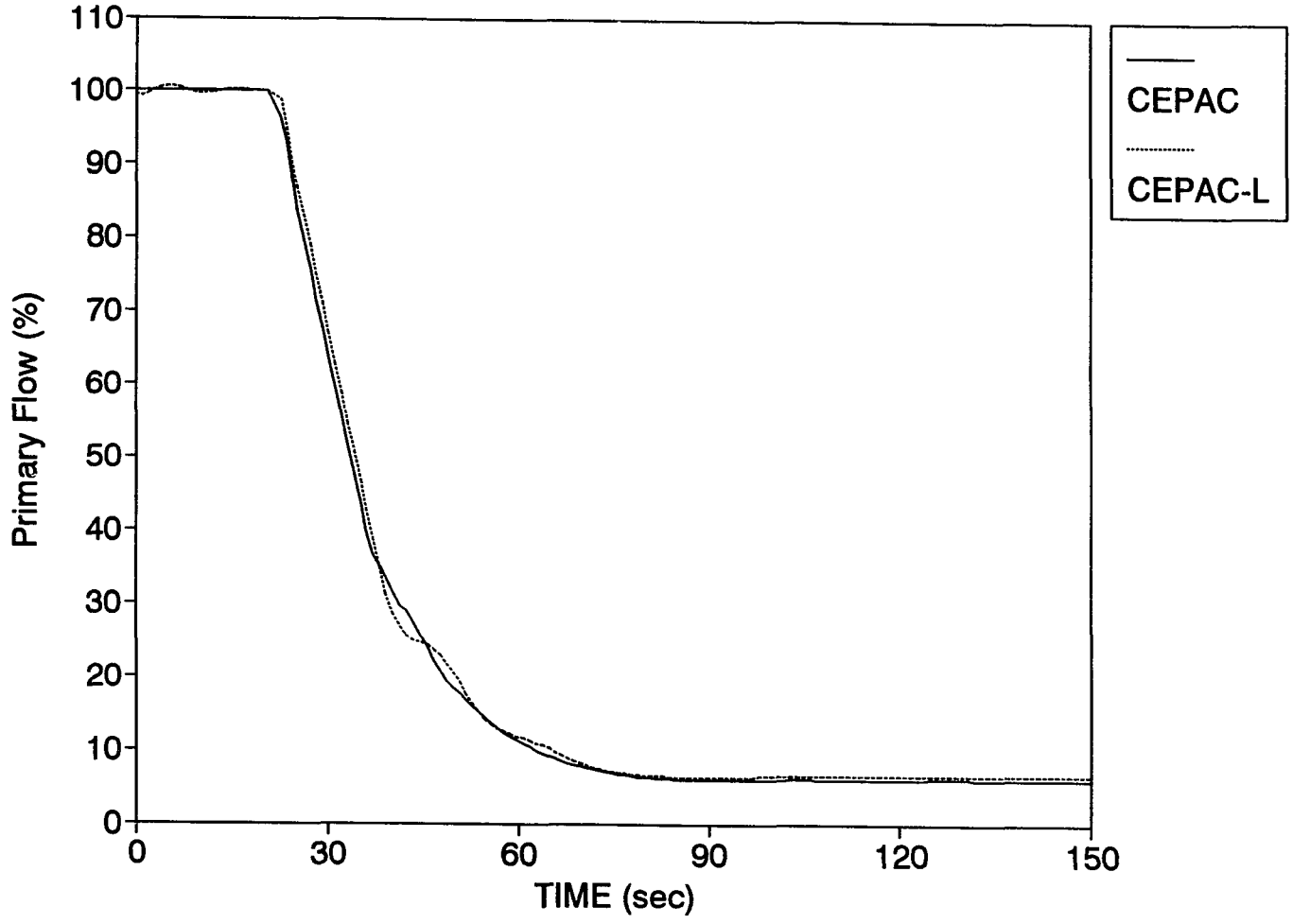

Figure 12. Primary Coolant Flow, Loss of All Flow

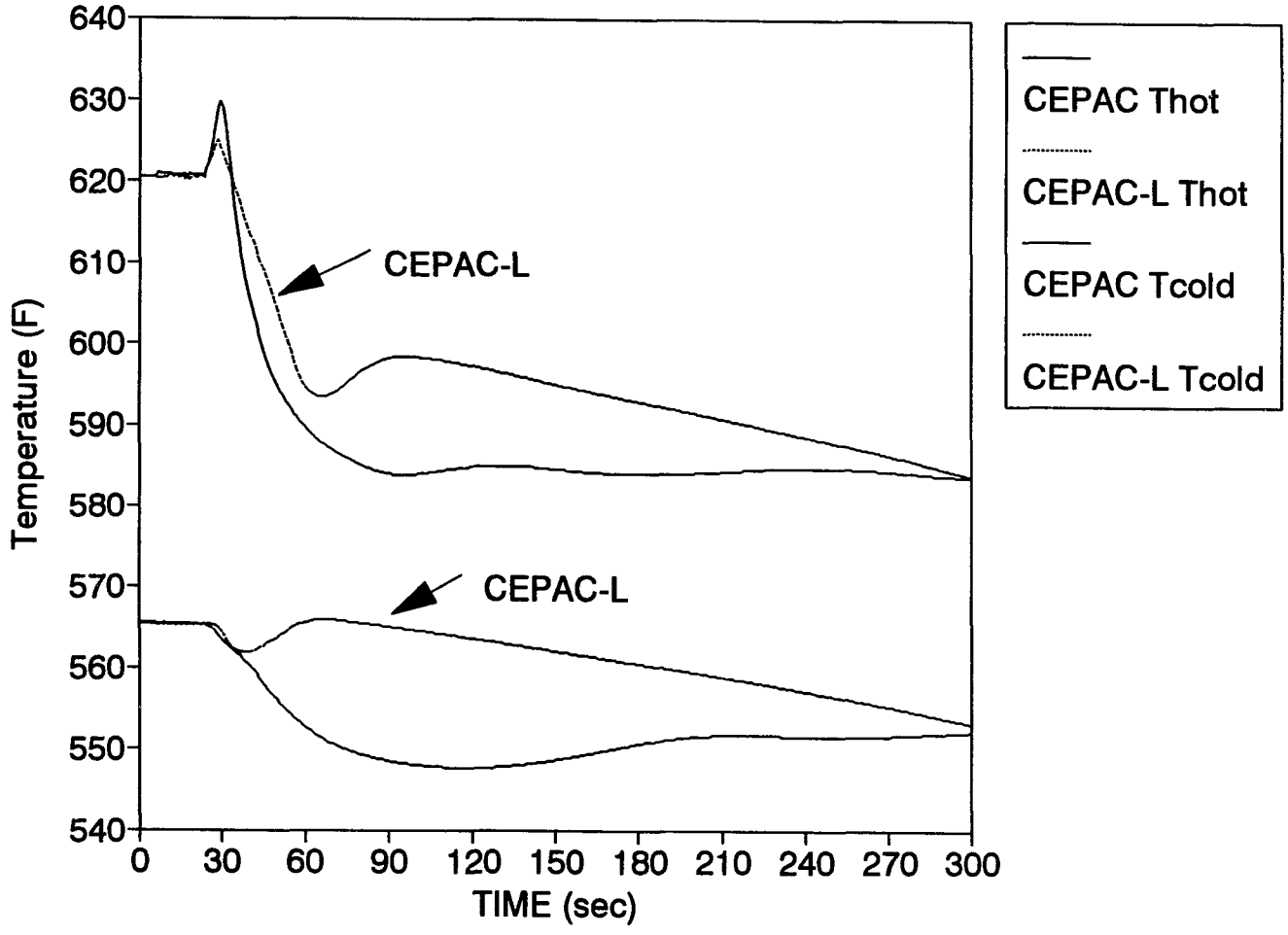

Figure 13. Loop Temperatures, Loss of All Flow

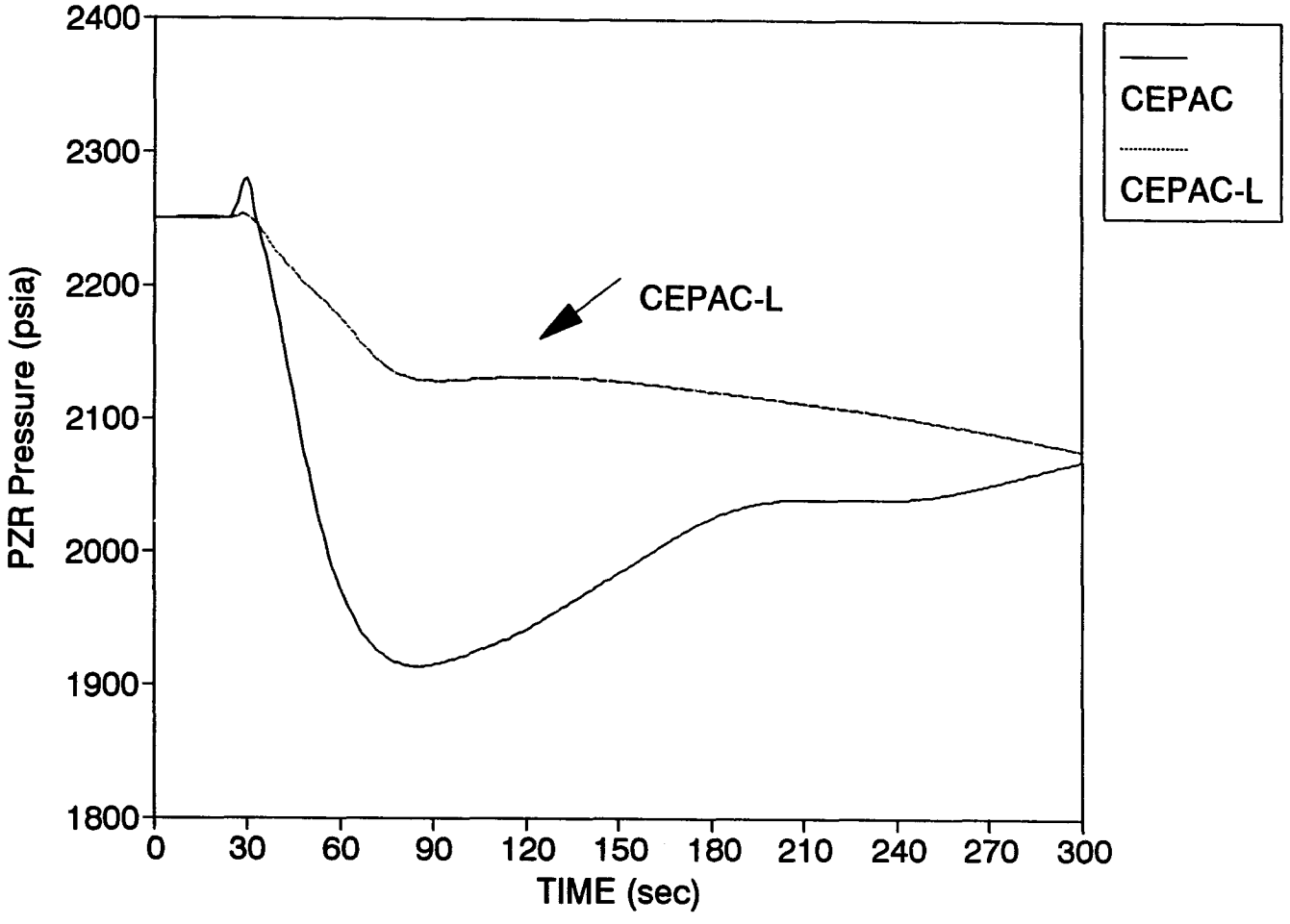

Figure 14. Pzr Pressure, Loss of All Flow

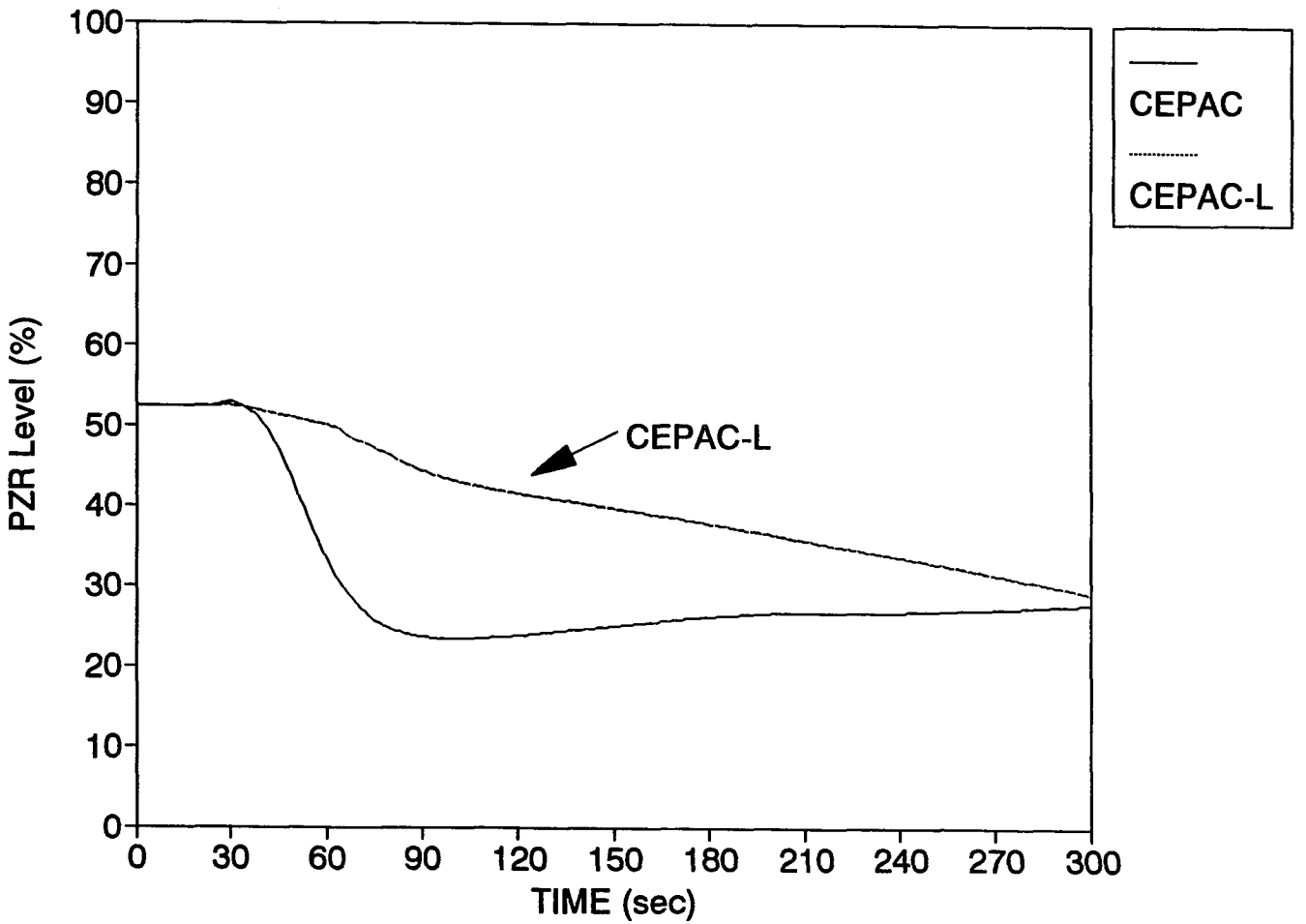

Figure 15. Pzr Level, Loss of All Flow

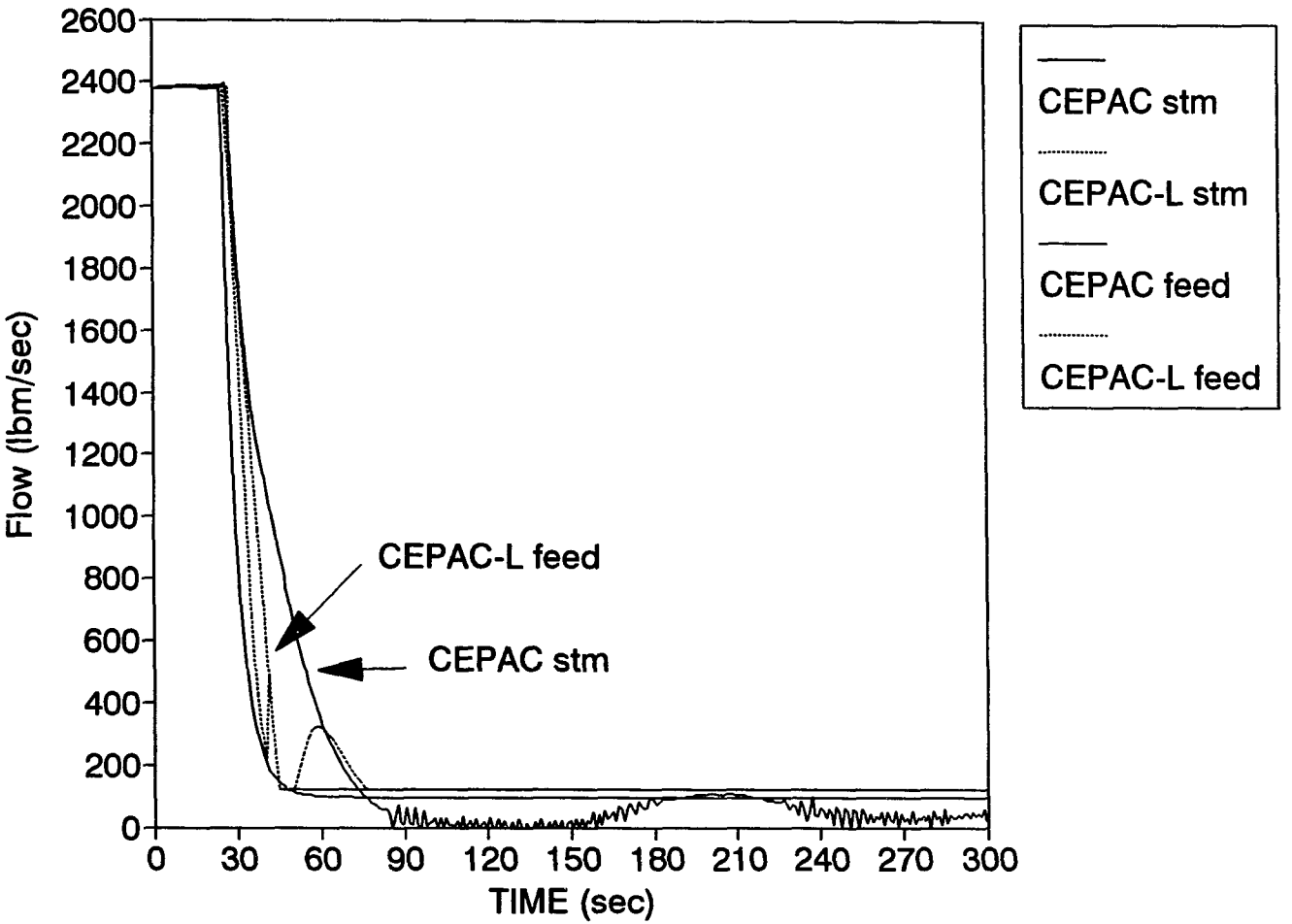

Figure 16. Steam and Feed Flows, Loss of All Flow

an immediate reduction in steam generator level setpoint. Once steam flow has been reduced to below the level of feed flow, at approximately 60 seconds, steam generator water level stabilizes at its new lower level as shown in Figure 17.

The CEPAC-L model shows an overall increase in steam generator water level due to the lack of a sophisticated feed water control system. In CEPAC-L feedwater flow rate and steam flow rate are exactly equal at around 60 seconds. However feed flow decreased at a slower rate than steam flow prior to that time causing the generator to be filled to over 85%. The higher final steam generator water level for CEPAC-L directly contributes to a higher steam generator pressure as shown in Figure 18.

Higher steam generator pressure and level caused by the lack of an accurate feed water control system in CEPAC-L also directly contributes to the smaller magnitude transients of pressurizer pressure, pressurizer level and loop temperatures. All three end up at approximately the same values that CEPAC predicts by 300 seconds.

Differences and inaccuracies in plant parameters between CEPAC-L and CEPAC occurred mostly due to a lack of sophisticated feedwater control and steam bypass control

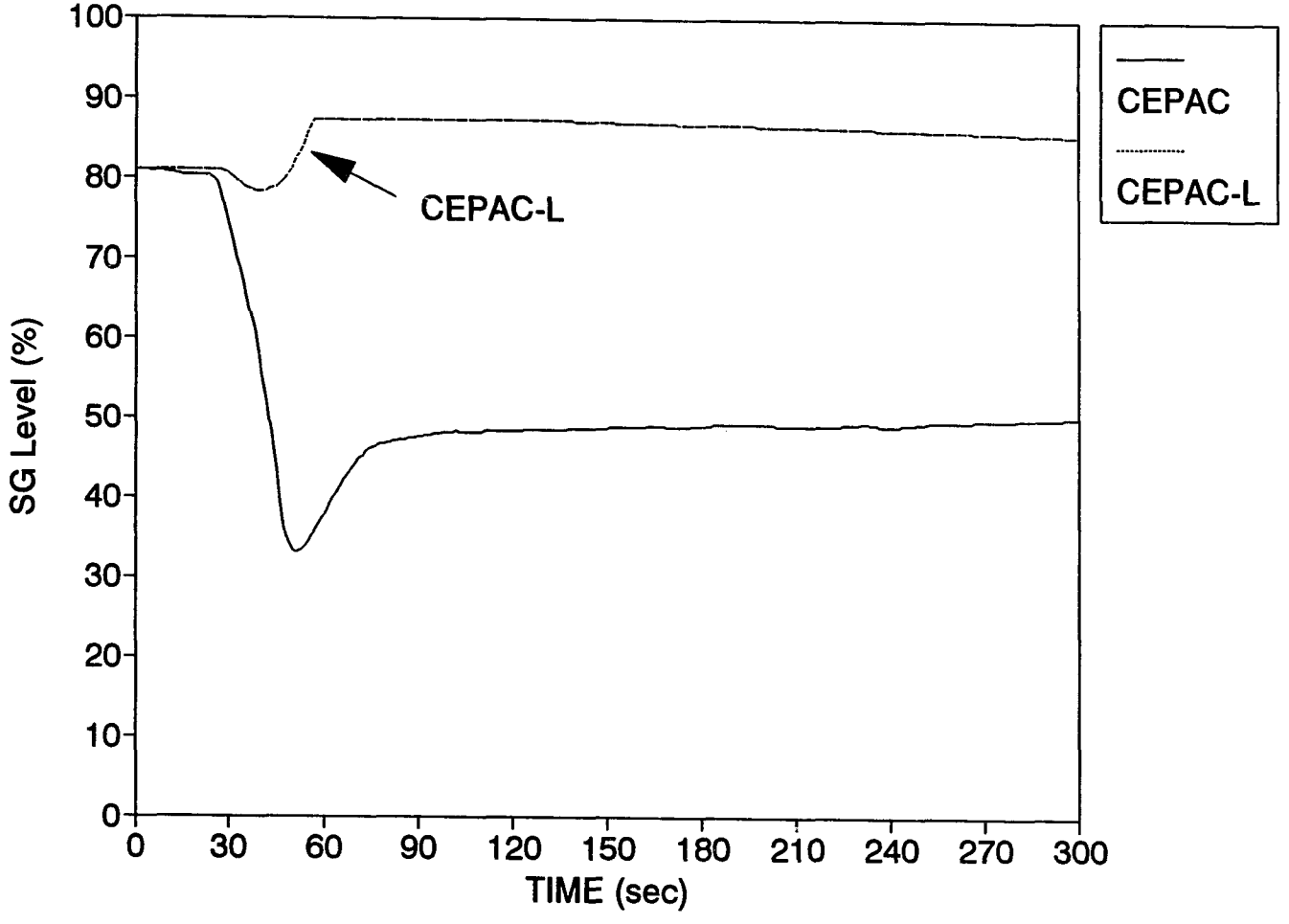

Figure 17. Steam Generator Level, Loss of All Flow

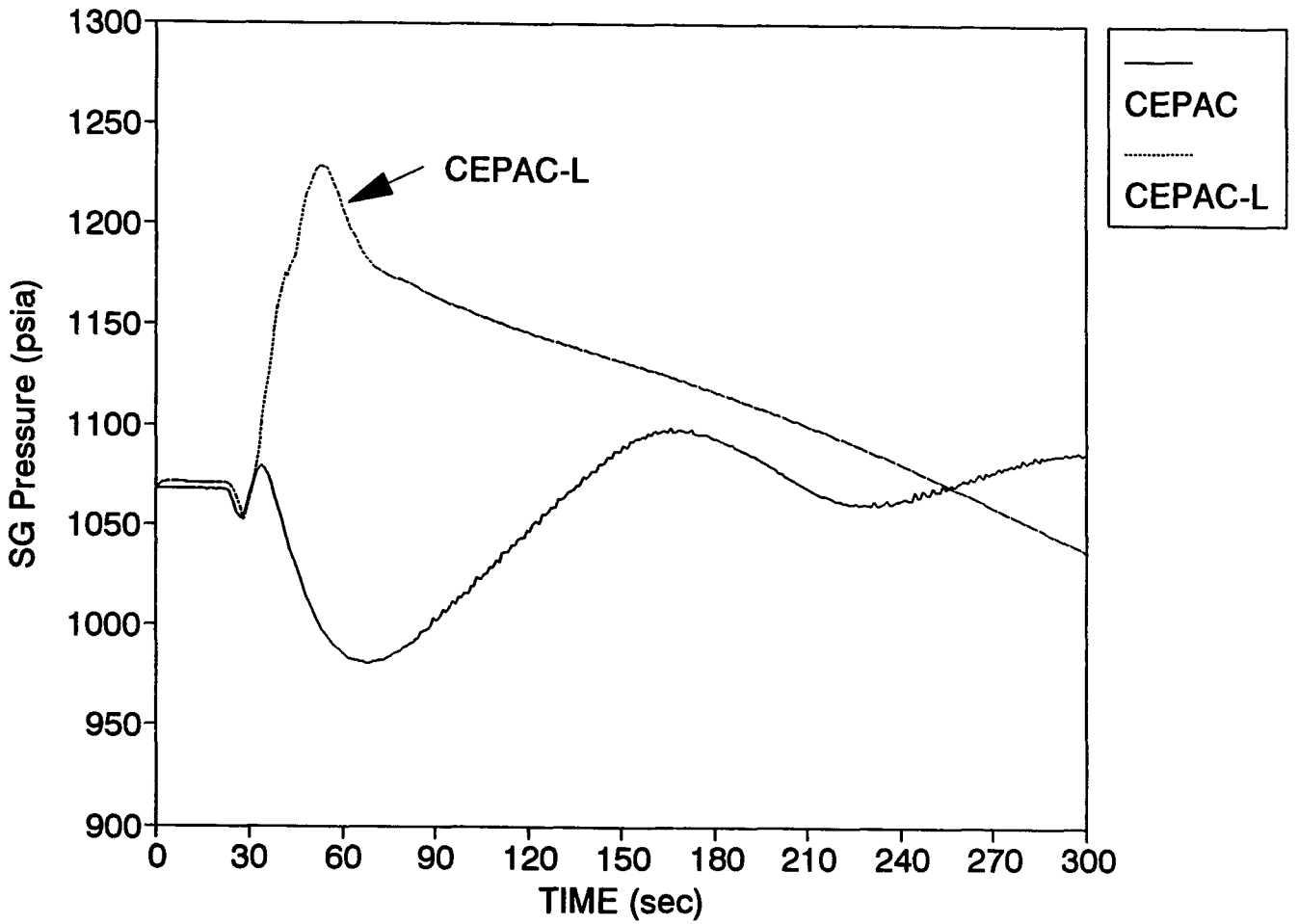

Figure 18. SG Pressure, Loss of All Flow

systems. The loss of all primary coolant flow transient as modeled by CEPAC-L does not fluctuate as severely in magnitude as CEPAC, but the parameters still track and are close to CEPAC values.

Comparison of FUELPIN to COBRA

COBRA used actual Palo Verde axial heat flux profiles for three times in core life, in addition to CEPAC-L pressure, inlet temperature and mass flux, to predict values and positions of MDNBR versus time for a Loss of All Flow transient. Axial heat profiles used are shown in Figure 19. For all calculations a radial peaking factor of 1.35 was used.

MDNBR versus Time.

For beginning of core life and end of core life heat flux profiles FUELPIN and COBRA have equal steady state values. Once reactor coolant pumps are tripped and the transient begins FUELPIN began to calculate values for MDNBR that were higher and therefore had extra thermal margin over COBRA. As shown in Figure 20, for beginning of core life FUELPIN predicts the lowest value of MDNBR during a LOAF to be 1.96 compared to a low value of 1.90 predicted by COBRA. Figure 21 shows for end of core life FUELPIN predicts the lowest value of MDNBR during a LOAF

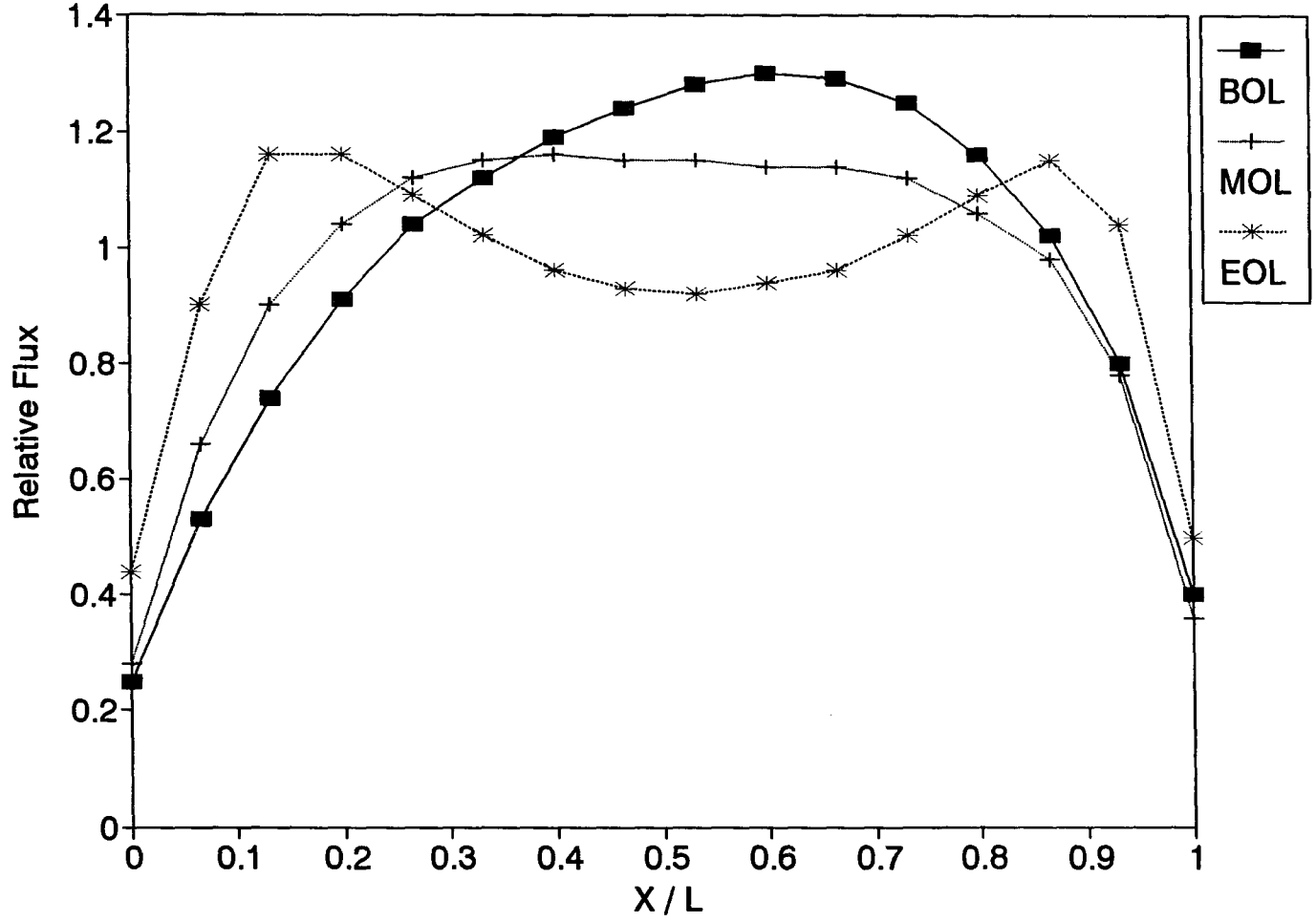

Figure 19. Axial Heat Flux Profile

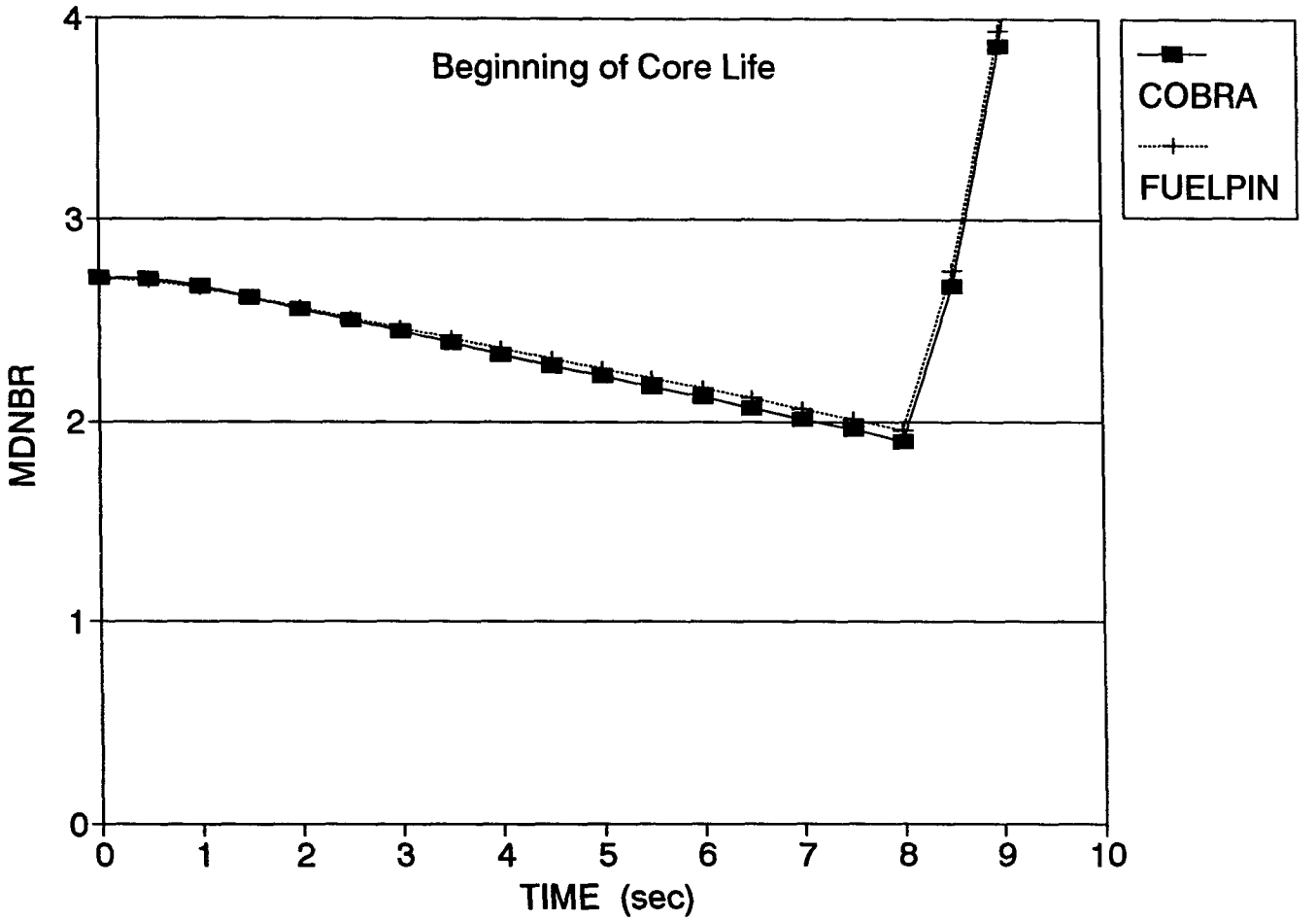

Figure 20. MDNBR vs Time, Loss of All Flow, BOL

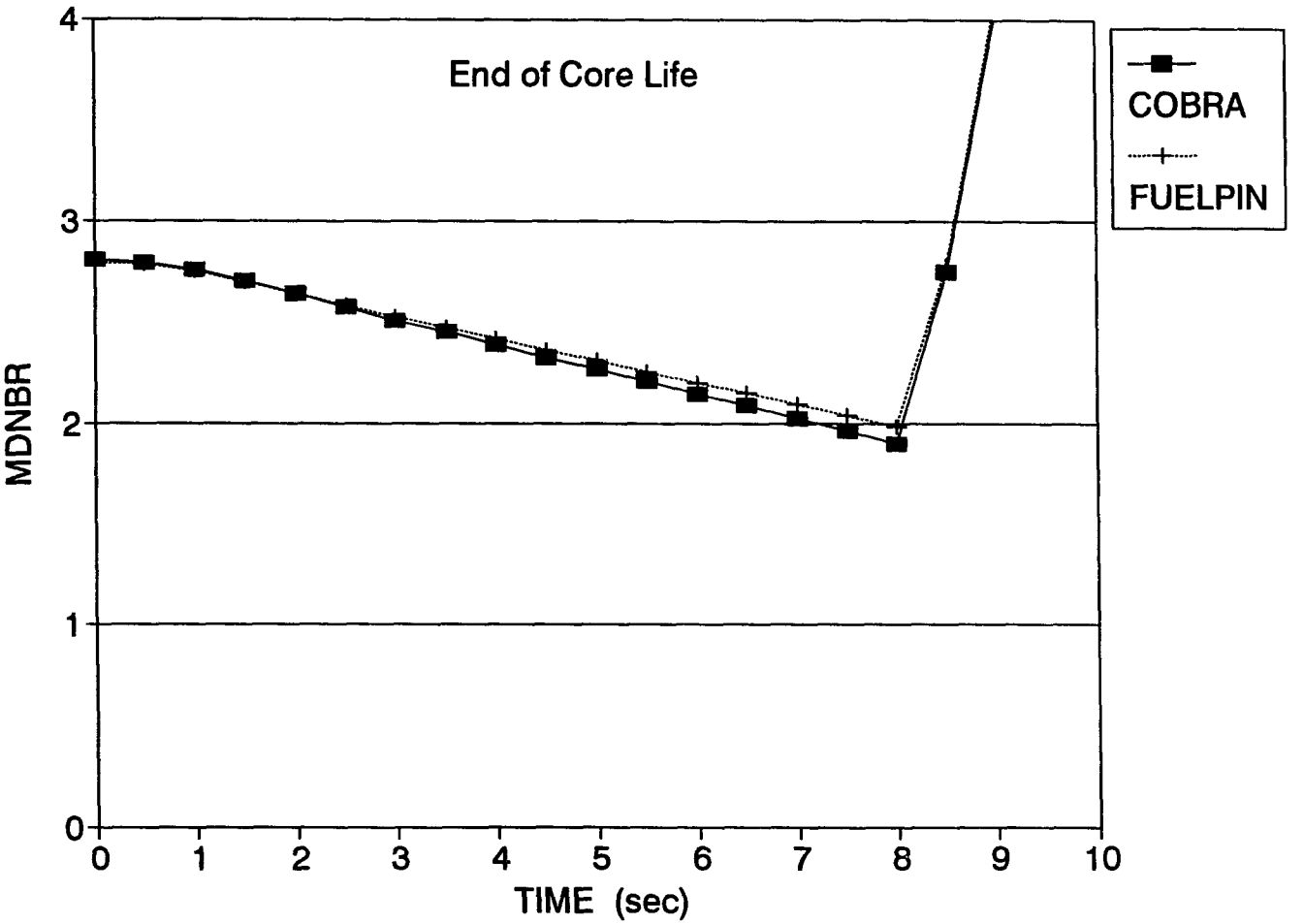

Figure 21. MDNBR vs Time, Loss of All Flow, EOL

to be 1.98 compared to a low value of 1.90 predicted by COBRA. The result is a gain of 3 to 4 % thermal margin.

This low value occurs just prior to the reactor scram when reactor power is still at a maximum but core flow is at 80%. The normal reactor scram value for low core flow is 95% at Palo Verde. This value was artificially lowered in CEPAC-L to get a longer transient for better comparison. After the reactor scram power and actual heat flux drop so rapidly that DNBR rises rapidly.

Higher values of MDNBR calculated by FUELPIN result from the fact that FUELPIN is a dynamic model while COBRA is a quasi-steady state model. The dynamic model accounts for a lag in time between an increase in fuel pin centerline temperature and an increase in moderator temperature. A quasi-steady state model will predict that a reduction in flow for a constant heat flux causes an immediate increase in moderator enthalpy which increases calculated actual heat flux and reduces DNBR.

A dynamic model accounts for the fact that an increase in fuel temperature will result in a lagged increase in moderator enthalpy due to the energy storage term in the general heat conduction equation. This means FUELPIN calculated values for actual heat flux will be lower than values predicted by COBRA. Therefore MDNBR values from FUELPIN will be higher than COBRA when the

scram occurs. Thus by FUELPIN calculations there is actually more thermal margin available than what COBRA is predicting.

The middle of core life heat flux profile results in a different transient (Figure 22). Steady state values for MDNBR are not equal. However, the same trend is evident in the transients. While FUELPIN predicted MDNBR at steady state is lower than COBRA, the lowest value reached prior to scram is equal. Once again the temperature lagging effect causes the transient as modeled by FUELPIN to be less severe.

Position of MDNBR versus Time.

Figure 23-25 are comparisons of predicted values for position of MDNBR versus time after initiation of a loss of all primary flow. Both models predict the same general trend of position of MDNBR during a transient. Since actual heat flux is a constant value until a reactor scram the only variable is critical heat flux. The heat flux necessary to achieve DNBR is decreasing throughout the channel as flow decreases. The closest point of approach between critical heat flux and actual heat flux, MDNBR, will occur later and later in the channel during the transient as temperatures increase. After the scram the position of MDNBR moves back toward the center of the

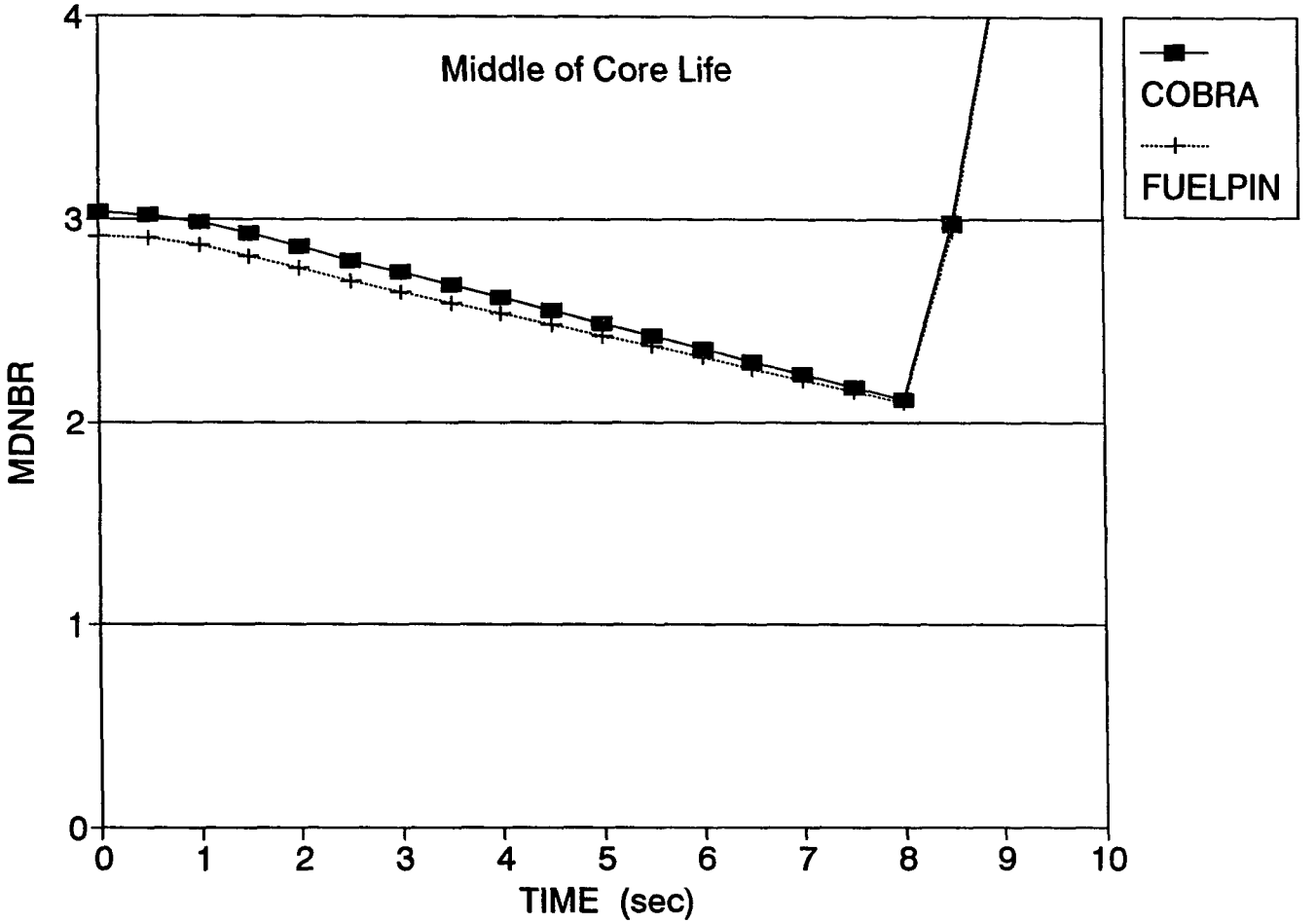

Figure 22. MDNBR vs Time, Loss of All Flow, MOL

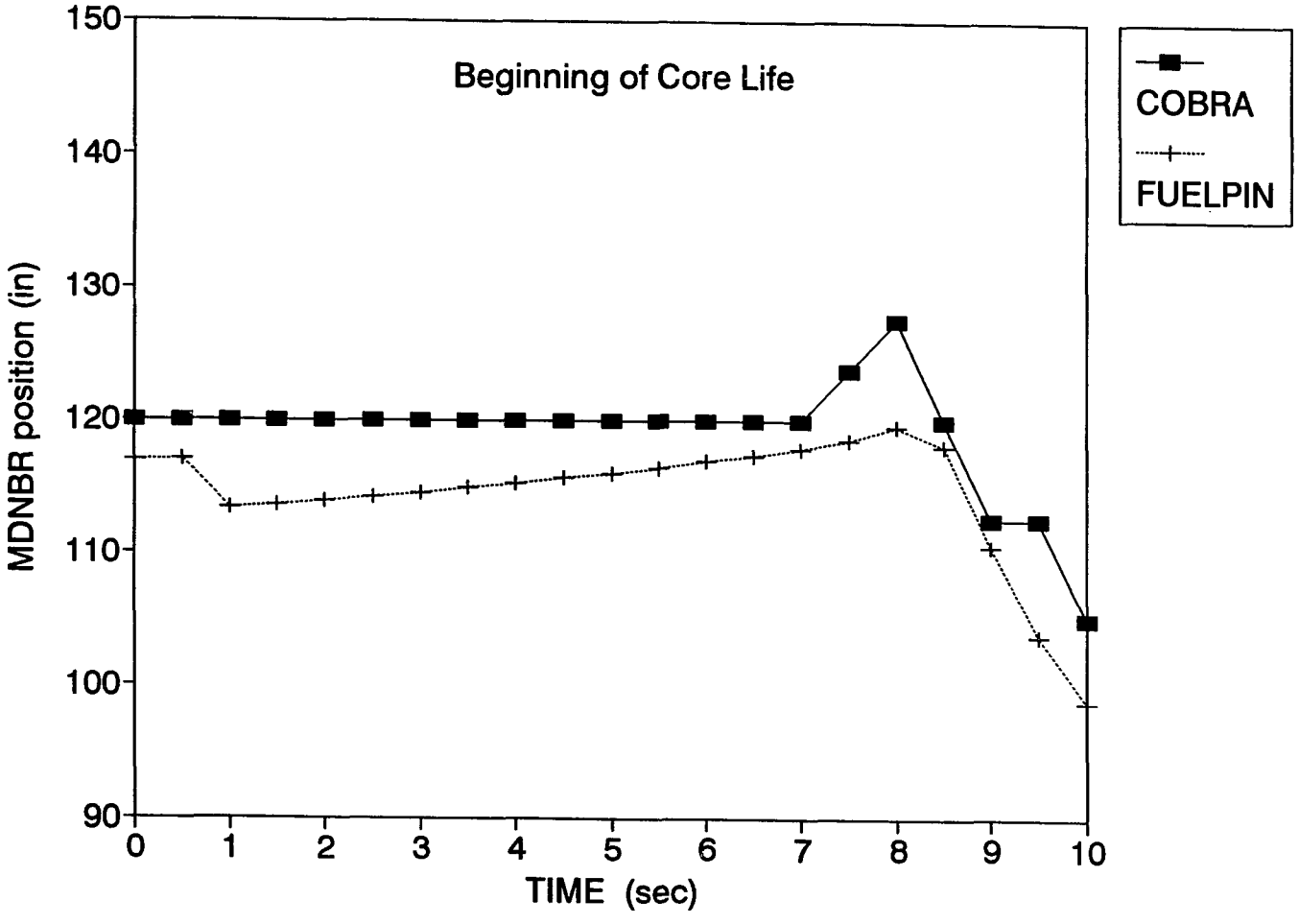

Figure 23. Position of MDNBR vs Time, LOAF, BOL

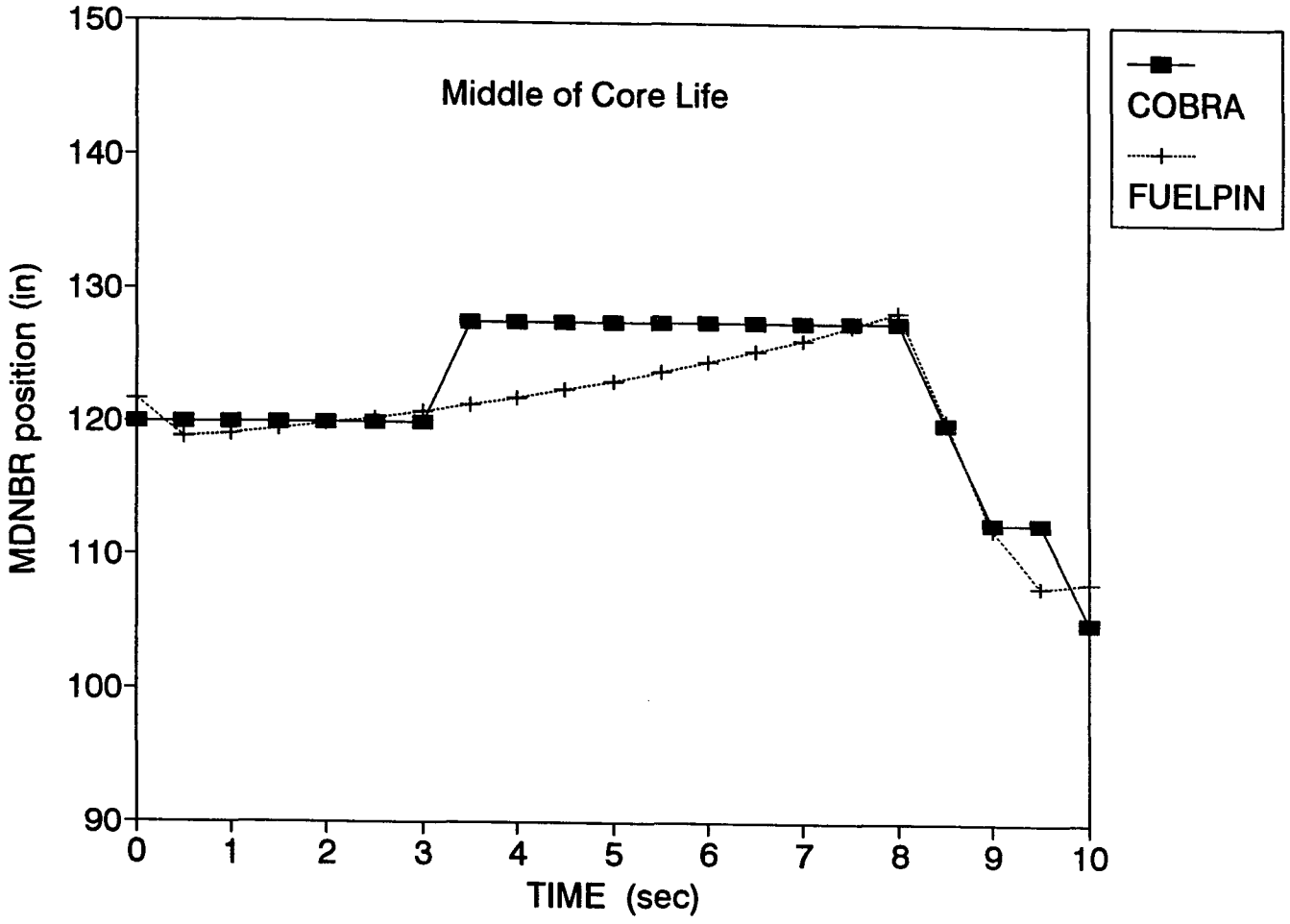

Figure 24. Position of MDNBR vs Time, LOAF, MOL

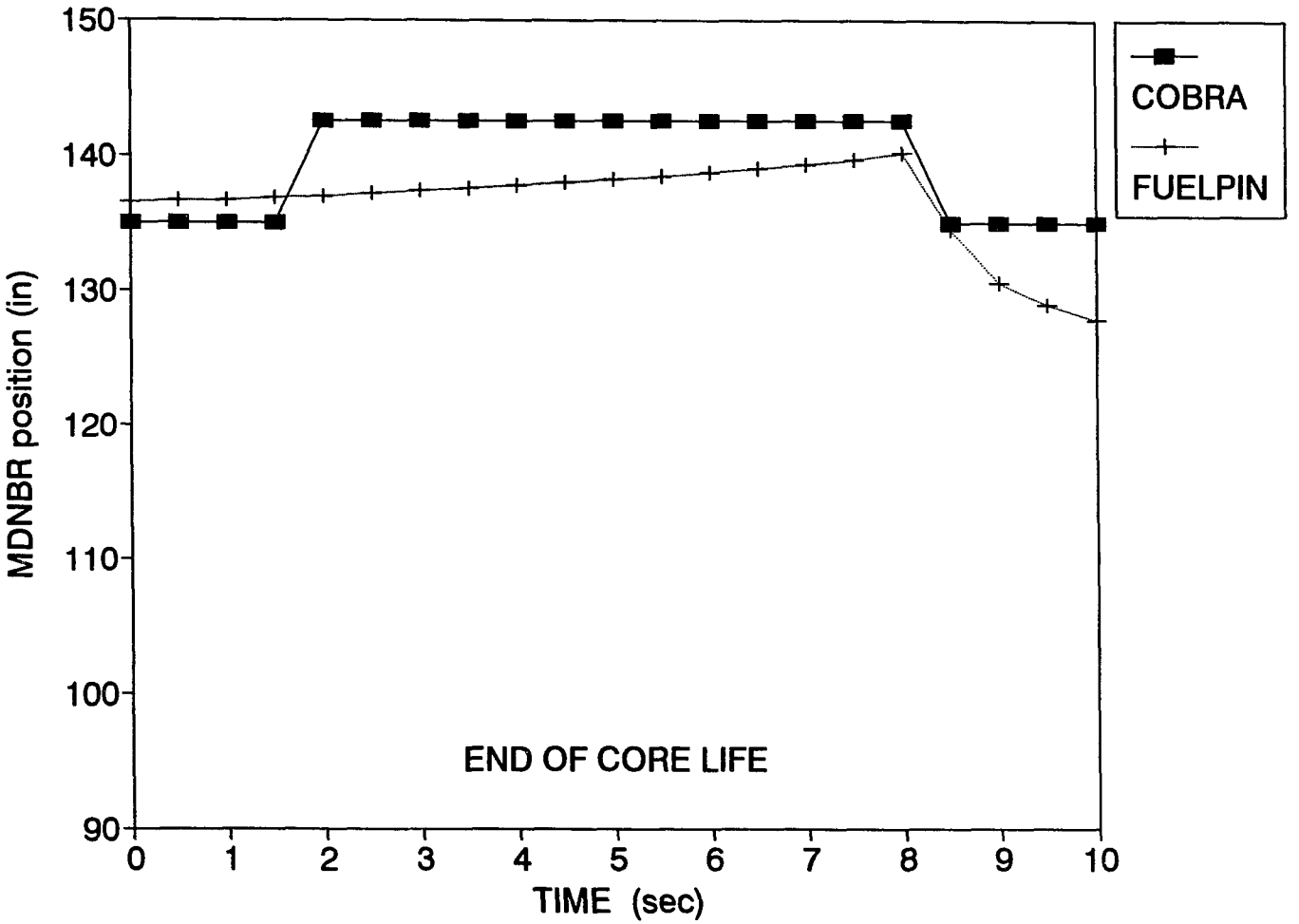

Figure 25. Position of MDNBR vs Time, LOAF, EOL

channel since actual heat flux decreases rapidly and becomes more uniform axially throughout the channel.

Over core life position of MDNBR moves toward the top of the channel due to flattening of the heat flux profiles caused by fuel burnup. This flattening results in higher heat fluxes at the end of the channel where moderator temperature is also highest.

The only significant difference between the curves at any time in core life occurs because COBRA uses 7.5 inch fixed nodes for its channel while fuelpin tracks the exact position of MDNBR.

DISCUSSION

The CEPAC-L model was shown to be an adequate representation of a PWR during steady state and a loss of all primary coolant flow casualty by comparison with CEPAC. CEPAC-L has two distinct features which make it ideal for use as a reactor plant simulation code:

1) It is coupled to LASAN and therefore has very user friendly input and output features.
2) It enables users to test new models of various components of a PWR by substituting or adding different modules.

Its most significant drawback is its lack of adequate models for a steam bypass control system and a feed water control system.

FUELPIN was shown to be a more complete model of the thermal hydraulics of a reactor fuel pin than COBRA. MDNBR predicted by FUELPIN resulted in greater thermal margin during transients for two reasons:

1) The code is dynamic and therefore accounts for temperature lag during transients.
2) The code does not neglect axial conduction.

In addition, the coupled use of simulation codes demonstrated by using CEPAC-L and FUELPIN together results

in a reduction in magnitude of uncertainties encountered when manually feeding one simulation code with output from another. It would be easy to incorporate this new fuel pin model into existing thermal hydraulic codes.

A code that predicts higher values for DNBR can be very valuable if it can be tested rigorously and accepted as an accurate standard. An increase in predicted values of MDNBR during anticipated operational occurrences would allow the core to be operated at higher powers without a reduction in thermal safety margins. If power level is not increased it would be possible to operate fuel assemblies for longer times allowing higher fuel burnup. Both higher power operation and extended fuel life could result in a large savings to nuclear power utilities. The FUELPIN model currently produces results that could ultimately lead to these kinds of savings.

APPENDIX A: CEPAC-L Module Causality Diagrams

This Appendix details the calculations performed by the modules of CEPAC-L and the interelationships between the modules.

REACTOR COOLANT SYSTEM (RCSLOP)

INPUTS	FROM
- Pressure	PRESZR
- Core power	KINET
- Mass gain/loss	UPPHD
	PRESZR
- Energy gain/loss	UPPHD
	PRESZR
- Trip signals	RPSYS

CALCULATIONS

- RCS node mass and energy balances
- RCS flow rates
- RCS temperatures
- RCS fuel temperatures
- Safety injection flow rate

OUTPUTS	TO
- RCS temperatures	UPPHD
	STMGEN
	KINET
	RRSYS
- RCS flow rates	UPPHD
	STMGEN
	RPSYS
- RCS pressures	UPPHD
- Surge line flow	PRESZR
- Fuel temperature	KINET

PRESSURIZER (PRESZR)

INPUTS	FROM
- Surge line flow	RCSLOP
- Trip signals	RPSYS

CALCULATIONS

- Region mass and energy balance
- PZR pressure
- PZR level
- PZR heater operation
- Spray valve operation and flow
- Relief valve operation and flow
- charging flow
- letdown flow

OUTPUTS	TO
- Pressurizer pressure	RCSLOP
	RPSYS
- Mass loss/gain	RCSLOP
- Energy loss/gain	RCSLOP

VESSEL UPPER HEAD (UPPHD)

INPUTS	FROM
- RCS flow rates	RCSLOP
- RCS pressures	RCSLOP
- RCS temperatures	RCSLOP

CALCULATIONS

- Flow rate to and from upperhead
- Region mass and energy balance
- Vessel pressure during leak

OUTPUTS	TO
- Mass gain/loss	RCSLOP
- Energy gain/loss	RCSLOP

KINETICS (KINET)

INPUTS	FROM
- Fuel Temperature	RCSLOP
- Moderator Temperature	RCSLOP
- Rod Position	RRSYS
- Trip signals	RPSYS

CALCULATIONS

1. Reactivity:
   - Fuel Temperature
   - Moderator Temperature
   - Rods
   - Boron
   - Total
2. Neutron density:
   - Fission neutrons
   - Delayed neutrons
3. Power:
   - Fission
   - Decay Heat

OUTPUTS	TO
- Core Power	RCSLOP
	RRSYS
	FEDWTR
	STMGEN

REACTOR REGULATORY SYSTEM (RRSYS)

INPUTS	FROM
- Core power	KINET
- steam flow to turbine	STMHDR
- RCS temperatures	RCSLOP

CALCULATIONS

- RCS average temperature (Tave)
- Error between Tave measured and program Tave
- Error between core power and turbine steam demand
- Total system error
- Rod speed and direction to control Tave

OUTPUTS	TO
- Rod position	KINET

REACTOR PROTECTION SYSTEM (RPSYS)

INPUTS	FROM
- Core power	KINET
- Pressurizer pressure	PRESZR
- Core flow	RCSLOP
- SG pressure	STMGEN
- SG level	STMGEN

CALCULATIONS

1. Reactor Trips:

   - High power
   - High pressurizer pressure
   - Low pressurizer pressure
   - Low core flow
   - Low steam generator pressure
   - Low steam generator level

2. Plant Trips:

   - Steam generator on reactor trip
   - HPSI system on at low pressurizer press
   - Main steam isolation on low SG press
   - Main feed isolation on high SG press

OUTPUTS	TO
- Trip signals	KINET RCSLOP PRESZR STMGEN STMHDR SBCS FEDWTR

STEAM GENERATOR (STMGEN)

INPUTS	FROM
- RCS temperatures	RCSLOP
- RCS flow	RCSLOP
- Core power	KINET
- Feed flow	FEDWTR
- Steam flows	STMHDR
- Auxiliary feed flow	FEDWTR
- Trip signals	RPSYS

CALCULATIONS

- Region mass and energy balances
- Steam generator pressure
- Heat transfer rate from primary to secondary
- Total steam flow

OUTPUTS	TO
- SG water level	FEDWTR RPSYS
- SG pressure	STMHDR RPSYS
- Total steam flow	STMGEN FEDWTR SBCS

STEAM HEADER (STMHDR)

INPUTS	FROM
- SG pressure	STMGEN
- Total steam flow	STMGEN
- Trip signals	RPSYS
- Steam bypass flow	SBCS

CALCULATIONS

- Steam header pressure
- Steam flow to turbine
- Safety valve flow

OUTPUTS	TO
- Steam header pressure	SBCS
- Steam flow to turbine	RRSYS

STEAM BYPASS CONTROL SYSTEM (SBCS)

This module is not represented in the CEPAC-L program. This diagram shows how the module would look in CEPAC.

INPUTS	FROM
- Reactor power	KINET
- Trip signals	RPSYS
- RCS temperatures	RCSLOP
- Steam header pressure	STMHDR
- Total steam flow	STMGEN

CALCULATIONS

- Steam bypass flow to prevent safety valve lift on reactor and turbine trips
- Steam bypass flow to prevent reactor trip on sudden load reduction

OUTPUTS	TO
- Steam bypass flow	STMHDR

FEEDWATER SYSTEM (FEDWTR)

This module is not represented in the CEPAC-L program. This diagram shows how the module would look in CEPAC.

INPUTS	FROM
- Core power	KINET
- Trip signals	RPSYS
- SG level	STMGEN
- Total steam flow	STMGEN

CALCULATIONS

- SG water level setpoint
- Desired flow rate
- Feedwater pump speed
- Downcomer valve position
- Economizer valve position
- Total feed flow
- Auxiliary feed system activation
- Auxiliary feed water flow rate

OUTPUTS	TO
- Total feed water flow	STMGEN
- Auxiliary feed water flow	STMGEN

REFERENCES

Arizona Nuclear Power Project system descriptions. (1984). Phoenix: ANPP.

CEPAC [Computer Program]. Combustion Engineering. Hans R. Van de Berg.

CEPAC-L [Computer Program]. Arizona Nuclear Power Project. Secker, P. A.

Chen, J. C., A Correlation for Boiling Heat Transfer to Saturated Fluids in Convection Flow. ISEC Process Design Dev., 5:322, 1966.

Groeneveld, D. C., An Investigation of Heat Transfer in the Liquid Deficient Regime, AECL-3281 (Rev) Dec 1968; Aug 1969.

Han,G. Y. (1993). A Mathematical Dynamic Modeling and Thermal-Hydraulic Analysis of Boiling Water Reactors Using Moving Boundaries. Unpublished doctoral dissertation, The University of Arizona, Tucson.

Incropera, F. P., and DeWitt D. P. (1981). Fundamentals of Heat Transfer, New York: Wiley & Sons.

Lahey, R. T. Jr., and Moody F. J., (1977). The Thermal Hydraulics of a Boiling Water Nuclear Reactor, La Grange Park, IL: American Nuclear Society

McDonough, J. B., Milich, W., and King, E. C., Partial Film Boiling with Water at 2000 Psig in a Round Vertical Tube, MSA Research Corp., Technical Report 62, NP-6976. 1958.

Rosenhow, W. M., and Dogall, R. S., Film Boiling on the Inside of Vertical Tubes with upward flow of the Fluid at low qualities, MIT-TR-9079-26, 1963.

Schrock, V. E., and Grossman, L. M., Forced Convection Boiling Studies, Final Report on Forced Convection Vaporization Project, TID-14632, 1959.

Secker, P. A., Jr., et. al., User's Manual for LASAN: A General Systems Analysis Code for Large-Scale Model Simulation, LATA Report GES-01-01, October 1979.

REFERENCES, continued

Thom, J. S., et al., "Boiling in Subcooled Water During Flow up Heated Tubes of Annuli", Proc. Instn. Mech. Engrs., vol. 180, part 36, 1966, pp. 226-246.

Todreas, N. E., and Kazimi M. S. (1990). Nuclear Systems I, New York: Hemisphere.

Tong, L. S., Heat Transfer in Water Cooled Nuclear Reactors. Nuclear Engineering Design, 6:301, 1967.

Webb, B. J., COBRA-IV PC Users Manual. Battelle-Northwest.